2009

High-frame-rate planar laser-induced fluorescence imaging of diesel sprays using pulse burst diagnostics

Joseph Fuller
Iowa State University

High-frame-rate planar laser-induced fluorescence imaging of diesel sprays using pulse burst diagnostics

by

Joseph P. Fuller

A thesis submitted to the graduate faculty

in partial fulfillment of the requirements for the degree of

MASTER OF SCIENCE

Major: Mechanical Engineering

Program of Study Committee:
Terrence Meyer, Major Professor
Song-Charng Kong
Hui Hu

Iowa State University

Ames, Iowa

2009

TABLE OF CONTENTS

LIST OF FIGURES

LIST OF TABLES

ABSTRACT

A planar laser-induced fluorescence technique for spatially and temporally resolving individual diesel fuel injection events into various gas temperatures and pressures was demonstrated. An optically accessible chamber of constant temperature and pressure was used to create the desired thermodynamic state of gas. The chamber was capable of achieving typical thermodynamic states seen at top dead center of the compression stroke in a four stroke diesel engine. The third harmonic of an Nd:YAG laser supplied excitation near 355 nm, which was provided at high frequencies using a pulse-burst diagnostic scheme. Individual pulses of 35 mJ in energy and 10 ns in duration were provided at rates of 10 kHz and 20 kHz. The UV laser beam was passed through a calibration cell filled with a laser dye, which was used for spatially correcting variations in individual laser pulses. The technique demonstrated that individual species concentrations can be temporally resolved using pulse-burst lasers.

CHAPTER 1. OVERVIEW

1.1 Background

Diesel engines today are one of the most ubiquitous sources of power in a wide variety of industrial applications. They are the engine of choice for many high power, high duty cycle applications due to high efficiency as well as relatively high torque output available at low engine speeds.

Although diesel engines perform a vital role in today's society, there are certainly many costs involved with their widespread use. One of the largest of these costs is air pollution. Compared to spark ignited engines, diesel engines typically operate at very high compression ratios. While thermodynamic efficiency is improved, high cylinder temperatures typically result. This, coupled with the sooting nature of diffusion flames, has led to traditionally high levels of both particulate matter and nitric oxides.

According to the Environmental Protection Agency (EPA), approximately 215 million people live in places where either particulate matter (PM) or Nitric Oxide (NO_x) levels can cause significant health problems which have been linked to premature death [1]. In order to combat this problem, the EPA began instituting a progressively stringent emissions reduction program consisting of "Tiers" [1]. Due to the significant reduction in allowable exhaust emissions for the Tier 4 level (2010), engine manufacturers have been aggressively pursuing technologies which have the capability to reduce overall emissions by more than 90 percent [1]. In order to achieve this goal, it is of paramount importance that engine designers have an intricate understanding of in-cylinder combustion processes.

1.2 Diesel Engineering

There are a wide variety of design parameters that affect the diesel combustion process. These parameters can be generally classified as either fixed or variable. Fixed parameters are those which would require mechanical modification to achieve, while variable parameters are those which can be adjusted during engine operation. Table 1 illustrates examples of both of these types of parameters.

Table 1: Examples of both fixed and variable engine design parameters.

Fixed Parameters	Adjustments
Air Handling-Intake	Filter Media/Design
	Manifold
	Intake Runners
	Throttle Cam Actuation
Air Handling-Exhaust	Exhaust Tube/Runners
	Aftertreatment System
	Muffler
Valvetrain	Camshaft
	Lifters
	Valve Springs
	Poppet Valve Design
Combustion Chamber	Compression Ratio
	Piston Design
	Combustion Chamber Type
Turbocharger	Turbocharger type
Fuel Injector	Fuel Injector Type

Variable Parameters	Adjustments
Exhaust Gas Recirculation (EGR)	Mass Flowrate
	EGR Temperature
Wastegate Position	Turbocharger Boost
Fuel Injection Logic	Injection Timing
	Injection Duration
	Injection Pressure
	Number of Injection Events

Naturally, Table 1 is not a comprehensive listing of fixed and variable parameters for all engine systems. It is intended to highlight the breadth of critical design parameters for

many diesel engine design systems. In fact, each of the parameter adjustments listed in Table 1 has a wide variety of design variations.

Although there are many variations in engine configuration, the design process can be somewhat simplified if it is looked at from a thermodynamic standpoint. With the exception of fuel injection, all of the parameters from Table 1 can be shown to affect charge preparation. Charge preparation refers to the thermodynamic state of the gaseous pre-mixture inside the cylinder prior to the injection of fuel. Examples of charge properties affected by design parameters include total mass, gas species composition, temperature, and pressure.

Once the charge preparation in a diesel engine has been achieved, the most significant parameter affecting combustion thenceforth is the fuel injection event. The choice of fuel injector coupled with the method of injection has a significant effect on both the performance and emissions output of a diesel engine. For this reason, the injection process has received a great deal of attention in recent years.

In order to study the effect of injection parameters, engineers have used a number of tools. Engine dynamometers, for example, have become a standard in both academic and industry applications. The effect of varying injection parameters can be readily observed using dynamometers, and the results obtained from dynamometer tests are highly representative of engine performance in the field.

Although dynamometers are useful engineering tools, the data generated by them does not typically provide visual information about the injection event. Understanding the link between visual injection dynamics and engine performance would be useful as an engineering tool for determining design changes that optimize the performance of the engine.

In order to image an injection event, it is necessary at minimum to have optical access to the spray. Due to the high velocity of a diesel spray, sophisticated camera equipment is also required. Because fast imaging techniques limit exposure durations, high powered light sources are generally required as well.

Because of the aforementioned imaging requirements, lasers have become increasingly popular as a diagnostic tool. Benefits of laser diagnostics as a spray characterization tool include high signal to noise ratios, high spatial resolution, and individual species viewing capabilities, to name a few [2].

Although there are numerous benefits to using laser techniques, there are certainly challenges to their application. Because optical access is required, experimental apparatuses are generally designed or modified to permit line of sight measurement. Due to the fact that combustion and spray studies often take place at elevated temperature and pressure, optical apertures containing fragile materials like fused silica must be designed with great care.

Beyond mechanical design requirements, there are also numerous other challenges. Some of these include laser tuning capabilities, spatial and temporal laser energy variations, optical alignment, event synchronization and timing, and general experimental uncertainty. Despite these challenges, researchers continue to display useful and wide-ranging benefits to using laser techniques for diesel spray and combustion studies.

CHAPTER 2. REVIEW OF LITERATURE

2.1 Scope

Because of the breadth of work performed by researchers in the past, it would not be prudent to review all applicable combustion research. The intent of the present review of literature is to highlight diesel spray and combustion research pertinent to the evolution of the present study.

2.2 Introduction

As previously stated, the byproducts of diesel combustion can include high levels of both soot and nitrogen oxides, especially at high loads. To improve the combustion process, it is desired to study the production of these chemicals at the visual level. One of the most useful tools for achieving this is the constant volume combustion vessel. The underlying purpose of a constant volume facility is to thermodynamically fix the state of a gaseous mixture in a diesel engine near top dead center of the compression stroke prior to the injection of fuel. Upon reaching the desired state, fuel is injected, and corresponding data is collected. Studies can be performed for a variety of purposes. Examples include spray penetration, vaporization, flame presence, and soot production. In a constant volume facility, there are generally no moving components contained within the system. The purpose of this type of work is to study the pure tendencies of a spray to react to a gaseous mixture of known properties. Phenomena of interest include, but are not limited to the propensity of a fuel to mix, pollute, diffuse, penetrate, evaporate, or ignite. Determination of the optimal conditions

for combustion can provide insight as to the best methods to use for diesel combustion on a larger scale.

Besides constant volume facilities, optically accessible engines have also been constructed with the intent of studying the combustion process on a larger scale [3]. This type of an apparatus has been shown to be an effective tool for the purpose of evaluating combustion in a dynamic environment. Imaging of single diesel jets in optically accessible engines, however, is somewhat limited.

2.3 Diagnostics

In order to perform non-intrusive studies of diesel sprays, a number of diagnostic techniques have been employed. The availability of a wide variety of tunable laser sources, as well as multiple dyes and tracers has allowed researchers to study nearly any molecule of interest [2, 4]. Typical quantities accessible by these techniques include soot concentration, liquid and fuel vapor distributions, and velocity field distributions. In many cases, these measurements can be performed simultaneously. By utilizing these techniques in a controlled environment, researchers have developed a far greater understanding of the fundamental processes that affect combustion.

2.3.1 Diesel Sprays

The fuel injection pressure in a typical diesel engine can exceed 150 MPa. At these injection pressures, the liquid fuel exits the nozzle at a highly turbulent velocity. Because of this, the formation and structure of the diesel fuel jet can vary greatly. Figure 1 illustrates the

structure of a typical diesel fuel injection event. The fuel spray of Figure 1 is comprised primarily of liquid fuel, which can be seen to break up towards the leading edge of the injection plume. The location of the fuel injector is indicated in yellow on the left side of the image. The evolution of the injection plume as combustion occurs has been examined more extensively by authors at Sandia Labs [5].

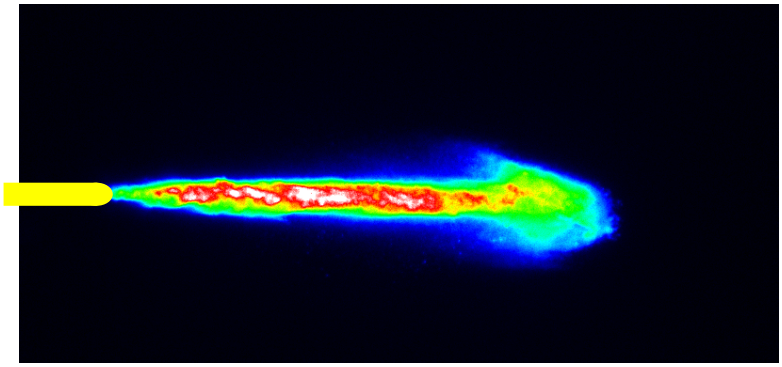

Figure 1: A typical diesel spray

Examples of variables affecting the jet structure include temporal fluctuations in fuel pressure, variable needle lift, and fuel injector orifice design. In order to characterize the jet formation and breakup process, as well as the spatial evolution of the spray, the spray structure has been measured by a number of methods for various designs. Examples of these techniques include laser anemometry [6], holography [7], schileren imaging [8,9], shadowgraphy [10,11], reflection and scattering [12-15], laser flow tagging [16], ballistic imaging [17,18], and x-ray imaging [19,20].

One of the most common metrics quantified by many of the aforementioned measurement techniques is penetration distance. This is due to the fact that it is a convenient

parameter for characterizing the global evolution of a spray. Researchers have used penetration distance measurements as a tool for developing and/or validating empirical models and correlations [8,13,21,22]. This has been a very widely studied value due to its dependence on a variety of experimental parameters. As an example, Morgan et. al. [23] have demonstrated significant dependence of penetration on nozzle geometry. Along with the potential to validate models and correlations, penetration distance has also been used as a parameter to characterize the development of the jet among various fuels under similar conditions [24].

Because of the highly variable nature of spray penetration, it is often convenient to study the velocity evolution as well. Phase Doppler Particle Anemometry (PDPA) has been shown to be an effective method for documenting momentum exchange in diesel sprays [25]. Although the velocity evolution of a spray is pertinent to the validation of models, supplemental data regarding the velocity distribution is often also desired. In order to achieve this, Particle Image Velocimetry (PIV) has been applied to diesel sprays [26]. PIV is a common diagnostic technique which is used to study the velocity field of a seeded flow. For the case of sprays, droplets are the "seeds" which are tracked via PIV search algorithms.

2.3.2 The Hydroxyl (OH) Radical

Although there are many species of interest in combustion diagnostics, the hydroxyl (OH) radical is by far one of the most common. This is primarily due to the fact that it exists in sufficiently high concentrations in hot regions of the combustion zone. As such, it is a reasonably good marker of flame presence. Excited state OH radicals are produced as a

consequence of a few key chemical reactions that take place during hydrocarbon combustion events [27]. Relaxation of OH molecules from the excited state causes the emission of photons, commonly referred to as chemiluminescence. In the absence of laser excitation, the so called OH chemiluminescence has been used extensively for establishing various metrics such the lift off length of premixed flames in diesel combustors [28-33].

2.3.3 Soot

The production of soot in diffusion flames is an extensively studied parameter. To reduce pollution, it is desired to understand conditions that produce high levels of soot. The constant volume vessel has been used as an effective tool for studying soot production in a controlled environment. Along with the OH radical, Pickett and others have characterized soot formation processes in lifted diesel flames using a constant volume vessel [27-32,34-37]. An extensive review of fuel properties affecting soot production was also presented by Svensson [38] and Tree [39]. Soot measurements have also been successfully demonstrated in optically accessible engines using laser absorption and scattering [40].

2.3.4 Laser-Induced Fluorescence

Laser induced fluorescence (LIF) is one of the most commonly used methods for exploiting the spectroscopic properties of molecules. Simply put, the fluorescence of a molecule or radical species consists of the absorption of energy followed by the spontaneous

emission of a photon. For LIF, energy is transferred into the species of interest via laser radiation.

Following the absorption of energy, the molecule is temporarily excited from its ground state to a state of higher electronic vibration energy. The relaxation of the molecule from the exited state to the ground state is accompanied by the emission of a photon. Figure 2 is a simplified diagram illustrating what is commonly known as the two-level model for the fluorescence of a chemical species. Fluorescence emission generally takes place on the order of 10-100 ns. Because of the short emission lifetimes, it is a convenient method for resolving high velocity media such as flames and sprays.

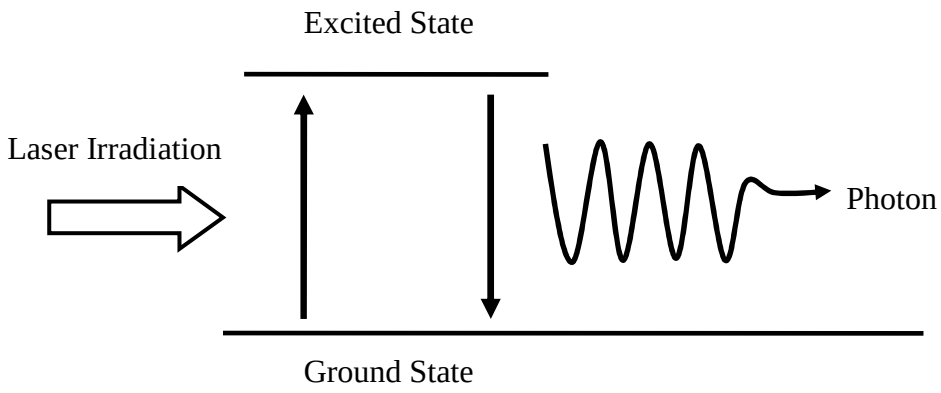

Figure 2: Simplified diagram of a fluorescence event.

Fluorescence studies generally involve a predetermined knowledge of the absorption and emission characteristics of the species of interest. Because this process has been well documented in the past, it is possible to experimentally determine molecular concentrations and spatial distributions.

LIF has a number of applications for both combusting and non-combusting sprays. A particularly simple and useful application of LIF is resolving concentration distributions, due to the fact that the measured signal intensity is proportional to the local species concentration.

2.3.4.1 Diesel LIF

Although fuels are assumed to consist of the same molecules for characterization purposes, they typically contain a wide variety of chemicals. The general purpose of these chemicals is to improve the performance of the fuel injection system or otherwise prolong the life of mechanical components [41]. Due to differences in climate and geographic location, diesel fuel composition can vary significantly. The variety of chemicals present in diesel fuel results in a broad absorption and emission spectrum. As such, a variety of ultraviolet excitation sources can be used for excitation of fuel sprays. Figure 3 is an example of the absorption spectrum for a sample of diesel fuel. As can be seen in Figure 3, a sample of #2 fuel oil tested at Iowa State University exhibited high absorption well into the UV spectrum, with a peak near 268 nm.

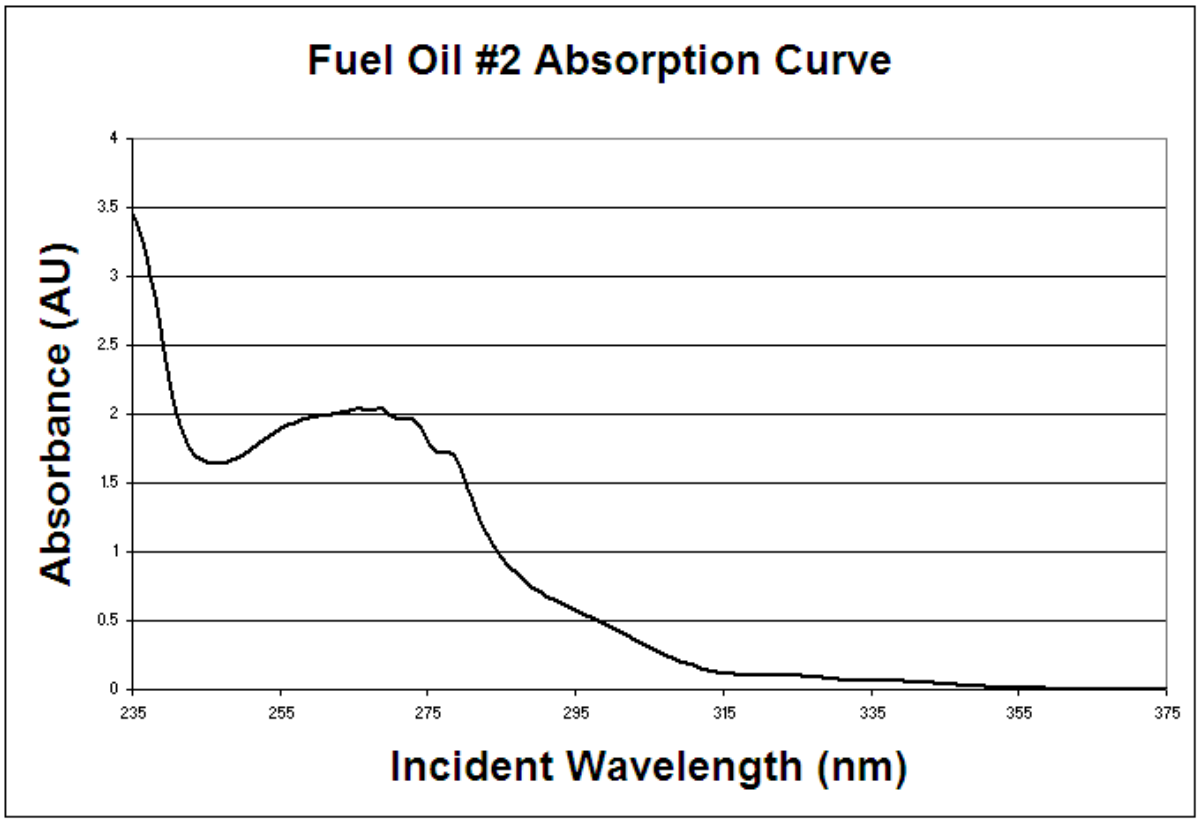

Figure 3: Absorption Curve for Diesel Fuel Oil #2.

Non-combusting diesel fuel injection events consist of a dense, high velocity flow field with many droplets. While various techniques such as shadowgraphy and laser elastic scattering have been used to aid in flow field visualization, recent LIF studies performed either exclusively or in combination with other measurement techniques have yielded promising results [42]. In previous experiments, the fluorescence signal in a liquid spray has been shown to be proportional to the volume of the droplets. Pending a normalization of the spatial distribution of the laser excitation source, as well as other parameters, researchers have generated planar laser-induced fluorescence (PLIF) data illustrating the ensemble averaged fuel concentration distribution of a diesel spray [43].

In addition to measuring the fuel concentration, techniques have been developed to measure droplet size distribution as well. Greenlaugh [44] has demonstrated once such technique which utilizes the geometric dependence of fluorescence and Mie scattering on droplet volume and droplet surface area, respectively.

Although most of the previously mentioned techniques are suitable for measurements with high spatial resolution, they are typically limited by repetition rate. In other words, most of the techniques can only provide one image per diesel injection event. As a result, tools have been developed for use at high frequency.

2.2.2.3 High-Frequency PLIF

Generally speaking, most laser sources used for fuel PLIF exhibit very short pulse durations. This is highly advantageous for studying diesel sprays, due to the fact that the fuel molecules will only emit photons for a short period of time following the absence of excitation. This allows the high velocity spray to be imaged with very high resolution, regardless of the camera exposure time. Although this is the case, the rate at which laser excitation pulses can be emitted with sufficient power is limited. This means that for most applications, the spray can only be imaged once per injection event.

Although turn-key high frequency lasers can be purchased, the energy output in the 10-20 kHz range is limited to the low millijoule per pulse range [45]. While this type of tool certainly has applications, the signal-to-noise ratio can be limited by the energy output. According to Smith and Sick, this is approximately the low energy threshold for quantitative fuel distribution studies [46].

In order to increase the available pulse energy, researchers have used an Nd:YAG laser cluster consisting of four Q-switched lasers in series [47-49]. While this method is effective as a diagnostic tool, the data collection is limited to eight images.

Recently, a method for producing high-frequency pulses in burst-mode operation was developed for high-speed flame and spray diagnostics [50-51]. The Nd:YAG pump laser used in the study is capable of generating pulses at frequencies high enough to permit diesel spray measurement. Furthermore, the available energy output per laser pulse is comparable to that of a commercial high-energy PIV laser. Finally, the energy available from this system permits sufficient pulse energies to be generated at a variety of output frequencies. This allows a variety of chemical species seen in diesel combustion to be viewed at high frequency.

CHAPTER 3. METHODS AND PROCEDURES

3.1 Objective

The main objective of the present study was to demonstrate a Planar Laser-Induced Fluorescence technique for spatially and temporally resolving high velocity diesel injection events. The technique was also intended to serve as a proof of concept for more advanced studies of high-frequency species concentration distributions. A general overview of the process used to achieve these measurements is presented in the current section.

3.2 Constant Volume Vessel Facility

A constant volume vessel was modified and refurbished in collaboration with John

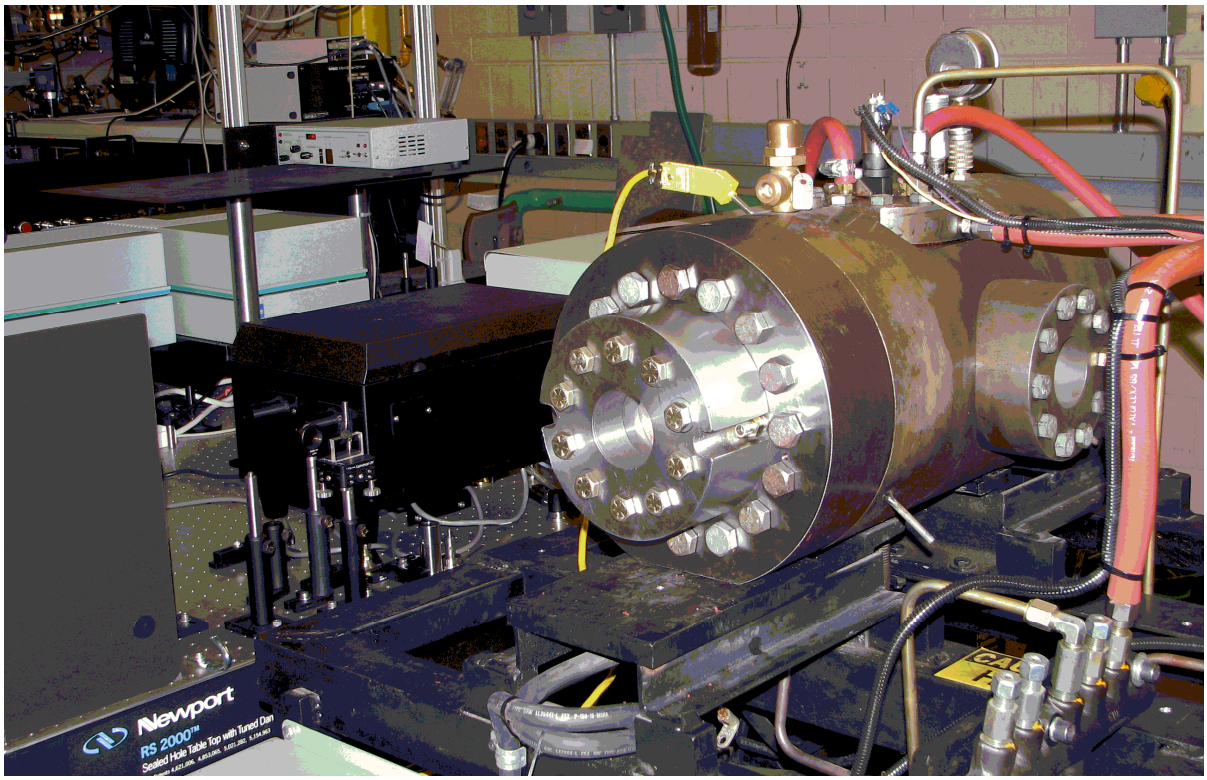

Figure 4: Constant Volume Combustion Vessel at Iowa State University.

Deere for use at Iowa State University. The vessel was modified to allow four points of optical access, two of which can be seen in Figure 4. The combustion vessel was used for imaging of non-combusting fuel injection events. There are a number of advantages to using a constant volume system to study diesel fuel sprays. Within structural limitations, nearly any thermodynamic state can be achieved in the vessel prior to fuel injection. In addition, the spray can be viewed unobstructed, which allows the injection event to be viewed with high spatial and temporal resolution.

3.1.1 Mixture Preparation

For elevated temperature studies, the gaseous pre-mixture was prepared by first heating the vessel to the desired temperature. Gas temperature was monitored using a thermocouple located approximately three quarters of an inch from the tip of the fuel injector, the signal of which was read into a temperature controller. The desired temperature was achieved and controlled using a PID control scheme. Using this method, gas temperatures near the fuel injector tip were observed to vary by approximately +/- 3 Kelvin from setpoint.

For atmospheric pressure studies, the chamber was purged with nitrogen prior to sealing. For elevated pressure studies, nitrogen was slowly fed into the chamber following purging and sealing. This allowed the chamber pressure to be modulated manually.

3.1.2 Fuel Injection Control

Typical diesel fuel injection takes place at very high pressure in order to facilitate rapid atomization of fuel. According to Borman et. al., the penetration distance L early in the fuel injection event can be approximated by,

$$\frac{L}{L_b} = 0.0349\left(\frac{\rho_a}{\rho_l}\right)^{1/2}\left(\frac{t}{d_0}\right)\left(\frac{\Delta p}{\rho_l}\right)^{1/2}$$

where L_b is breakup length, ρ_a is ambient air density, ρ_l is liquid fuel density, d_0 is injector orifice diameter, Δp is the pressure differential across the injector, and t is time. Using this equation, the average velocity of fuel droplets was estimated using the quantity L/t. For the injector at hand, fuel droplet velocities were expected to be on the order of 50 – 200 m/s near the injector tip. Due to the high velocity, it was essential to utilize an injection control scheme with high temporal resolution. In order to investigate the limits of injection timing control, two separate methods of fuel injection control were used. These consisted of a manually controlled injection system and engine module controlled system.

3.1.2.1 Externally controlled injection

The advantage of externally controlling fuel injection without a commercial engine control module was that the timing and duration of fuel injection events could be directly modulated using a Stanford Instruments model DG535 function generator. Since the instrument has high resolution and low jitter, the relative amount of uncertainty present from a data acquisition standpoint was minimized. The main drawback to this system was the fact that the overall fuel injection quantity and rate were unknown.

3.1.2.2 Engine Module Control System

As previously mentioned, an external industrial engine control module was installed on the periphery of the combustion vessel rig. This type of module is normally installed on production diesel engines. As such, inputs were provided via the data acquisition system in order to simulate engine operation and allow on-demand injection. The primary function of the engine control module was to monitor and control the fuel system as specified by the user. Variable input parameters included, but were not limited to:

- Total fuel injection quantity
- Common Rail Fuel Pressure
- Main fuel injection timing
- Pre-injection events, quantity and timing

The advantage of the engine module injection system was that it could be considered representative of typical injection events in production engines.

For both injection systems, a similar method of triggering was used. The methodology implemented for the synchronization of laser pulse, camera shutter, and fuel injection is illustrated in Figure 5.

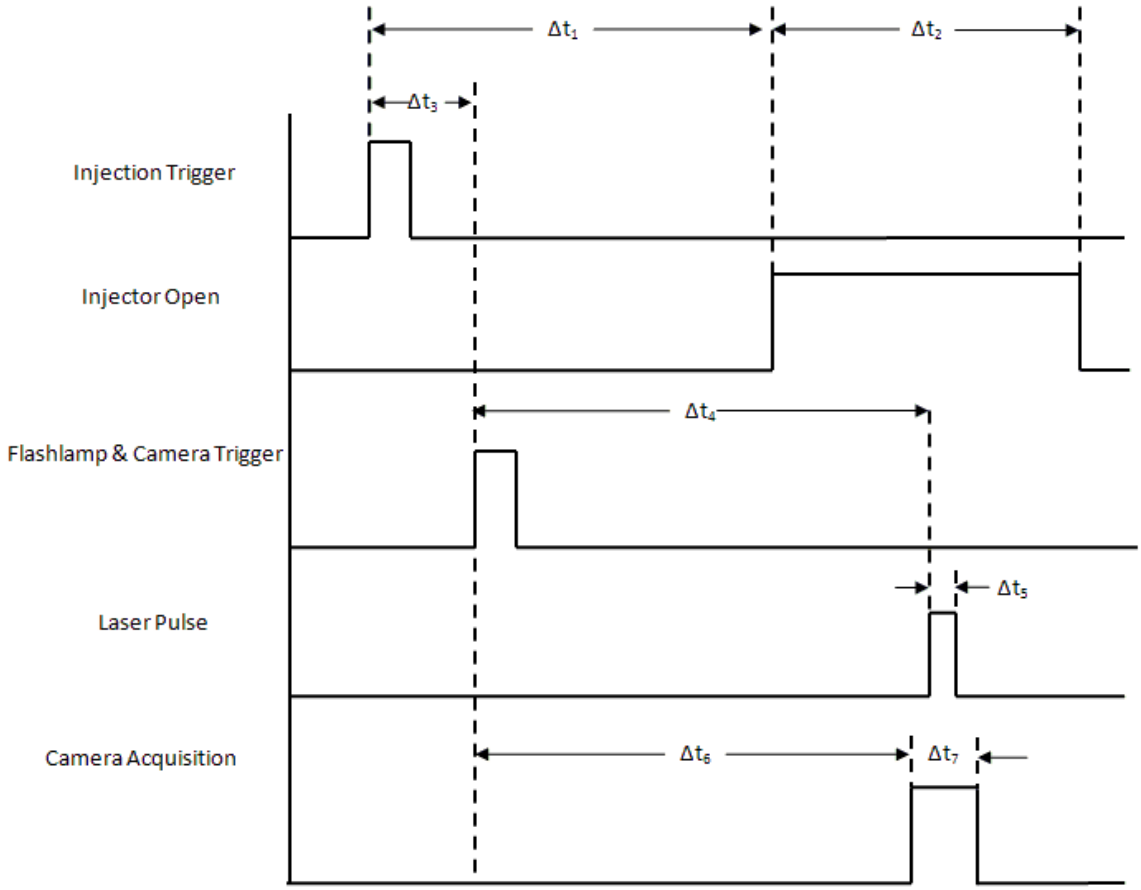

Figure 5: Timing scheme used for the synchronization of events.

Details of the timing system shown in Figure 5 are as follows:

Δt_1 = The nominal delay between the injection trigger and the onset of fuel flow. This value was observed to vary from 500-1100 us, depending on the gaseous pressure inside the constant volume vessel.

Δt_2 = Fuel injection duration. This value was adjustable from 500 to 2500 us. Using the engine control module injection system, injection duration varied depending on the desired fuel quantity and fuel injection pressure.

Δt_3 = Delay between injection triggering and laser flashlamp/camera triggering. Adjustment of this value determined when data was captured with respect to the start of injection (SOI).

Δt_4 = 180 us nominal delay between the flashlamp trigger and corresponding laser pulse.

Δt_5 = 10 ns nominal laser pulse duration.

Δt_6 = Internally adjustable camera delay. This value was set to coincide with the laser excitation pulse.

Δt_7 = Adjustable camera shutter duration.

3.3 Preliminary Experimentation

Preliminary experimentation was conducted utilizing the output of a commercial Q-switched Nd:YAG laser. The laser generated pulses of approximately 10 ns in duration at a repetition frequency of 10 Hz. This type of laser was used for single-shot measurements due to the fact that the startup, shutdown, and power output level of the system was easily manageable during initial experimentation. For all planar images, the laser profile was formed into a collimated sheet which measured approximately 45 mm in height and 300 um in thickness at the injector tip.

As previously shown in Figure 3, diesel fuel #2 has high absorption near 268 nm. For this reason, it was suitable to use the fourth harmonic of the Nd:YAG laser near 266 nm for excitation for the preliminary experimentation.

A commercially available PIV camera was used for preliminary studies. The 12-bit camera resolution was 1024x1280 pixels. To utilize the dynamic range of the CCD array, the

laser was passed through the spray at sufficiently high excitation energies. Increasing amounts of light were then let into the camera until the maximum observed image energy was near half of the saturation limit.

The raw images were processed by subtracting the light seen from ensemble-averaged background and scattering images. The penetration distance value for each injection event was calculated using MATLAB. Figure 6 is a sample of the centerline signal intensity of a typical injection event. The penetration distance was calculated by determining the location where the signal intensity dropped below a pre-determined value.

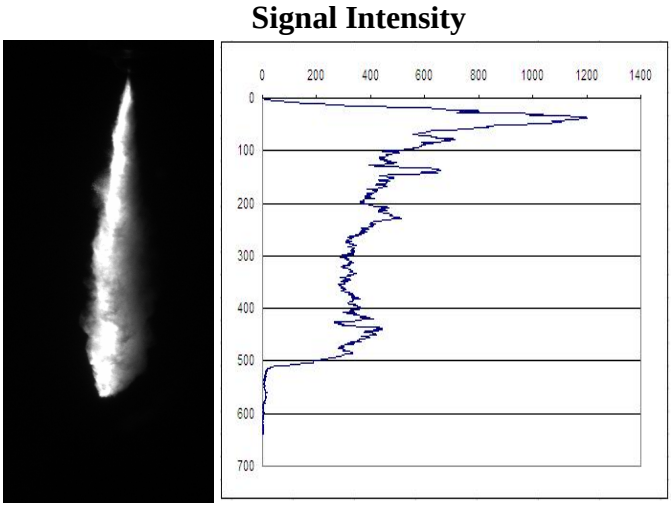

Figure 6: Methodology for penetration distance calculation.

For all experimental setups, a resolution grid was used to determine relative distances. Figure 7 shows the grid configuration used for the determination of penetration distance.

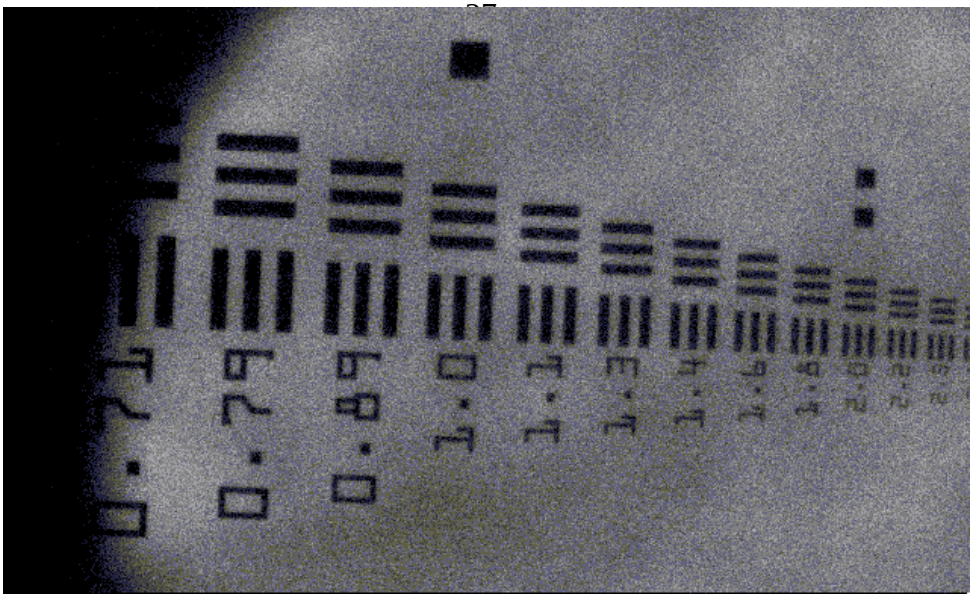

Figure 7: Resolution Grid used for determination of penetration distances.

3.4 High Frequency Experimentation

High-frequency images were acquired using a similar optical setup to that described in the preliminary experimentation. The laser source for this case, however, was a custom built pulse-burst laser diagnostic system [41-42]. The system was capable of generating 1 ms long pulses with bursts at rates of up to 100 kHz. For the present study, tests were performed at burst frequencies of 10 kHz and 20 kHz. Although more power was available, each discrete laser shot within a given burst train was tuned to emit approximately 35-40 mJ over a 10 ns duration. Figure 8 illustrates the pulse configuration in greater detail.

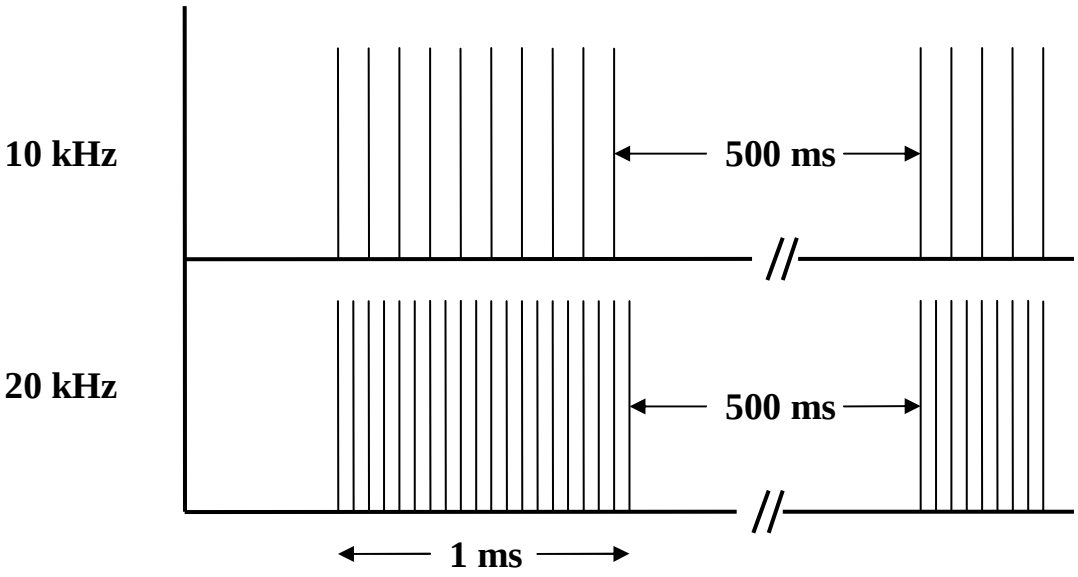

Figure 8: Pulse-Burst train timing configuration for 10 kHz and 20 kHz rates.

As shown in Figure 8, the number of laser shots increased as the burst frequency increased. Although the higher burst frequency yielded a higher temporal resolution, the spatial resolution was reduced. This was due to the speed-tradeoff property commonly encountered with the use of high frame rate cameras.

Because laser systems generally exhibit both spatial and shot-to-shot variability in energy output, it was necessary to apply corrections to raw images. In order to apply these corrections, a calibration cell was used for determining variations in laser energy. The cell was filled with a calibration fluid, and the laser sheet was passed through the cell prior to the spray. To prohibit damage to the materials, the cell was placed outside of the constant volume vessel.

In order to simultaneously acquire the calibration and spray images, four broadband reflective mirrors were used. This allowed the calibration cell and spray to be imaged onto

the CCD array of the same camera. Figure 9 is an image of the experimental setup used to accomplish this.

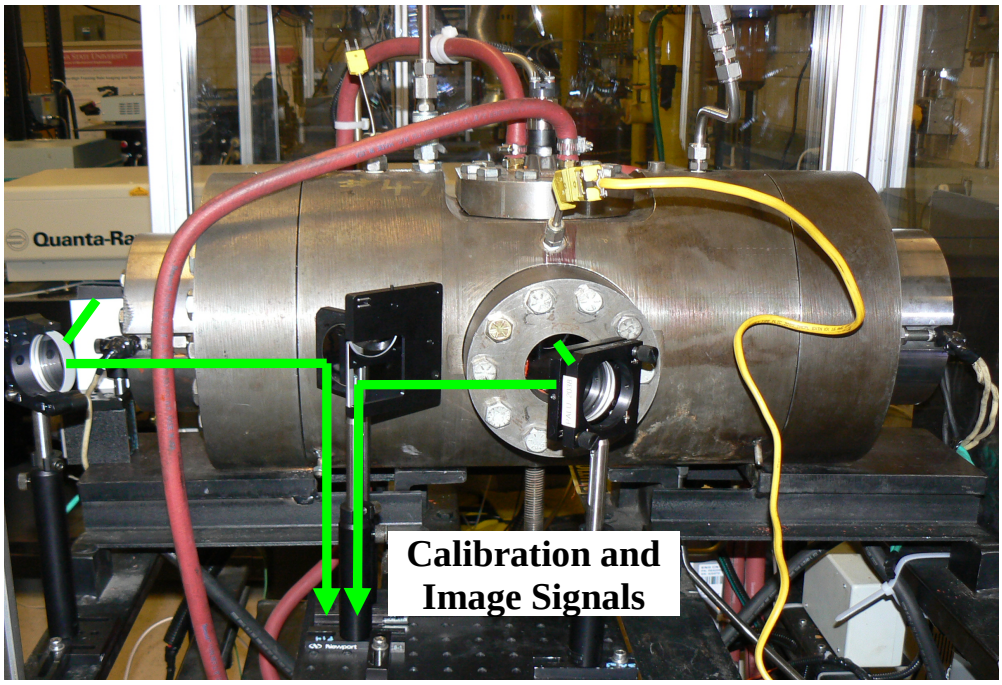

Figure 9: Optical setup for simultaneous imaging of calibration signal and spray image.

The green colored lines seen in Figure 9 illustrate the optical path traveled by the calibration cell and spray image. Keeping both images in focus necessitated that the light from the calibration cell and spray image travel the same distance prior to entering the camera.

CHAPTER 4. RESULTS AND DISCUSSION

4.1 Preliminary Results

The results from preliminary experimentation are presented in the current section. First, the shot-to-shot variability in injection timing was assessed. Due to the high velocity of the diesel sprays, it was necessary to minimize shot-to-shot variations in injection timing in order to minimize error. Second, photophysical properties were investigated for the diesel fuel used in the study.

4.1.1 Injection Timing Variability

Injection events were recorded for each of the setpoints shown in Table 2. This table of setpoints was run for both the manual and engine control module injection methods.

Table 2: Injection Variability Test Setpoints, Manual and Engine Module Injection Methods

Setpoint No.	Fuel Injection Pressure (MPa)	Absolute Ambient Gas Pressure (kPa)	Number of Injections	Ambient Temperature (K)
1	90	101	25	300
2	90	3550	25	300
3	110	101	25	300
4	110	3550	25	300
5	130	101	25	300
6	130	3550	25	300
7	150	101	25	300
8	150	3550	25	300

For each of the setpoints taken at 101 kPa, the penetration distance was evaluated over 25 separate injection events at 25, 75, 125, and 175 microseconds after the start of

injection (ASOI). Figure 10 is an illustration of four representative images taken at various times after start of injection.

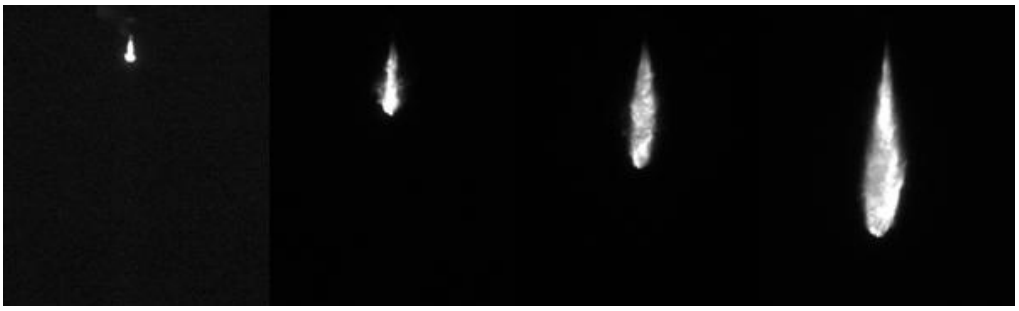

Figure 10: Sequence of Injection events at 25, 75, 125, and 175 us ASOI into nitrogen @ 1 atm

The images shown in Figure 10 were performed at 90 MPa injection pressure into Nitrogen at 1 atm.

For injections into high pressure gas, the spray was observed to penetrate significantly slower due to the increased gas density. As such, penetration distance for elevated pressure studies was evaluated at 50, 250, 450, and 650 microseconds after the start of injection. Figure 11 is an illustration of spray penetration into nitrogen at 3550 kPa at 90 MPa injection pressure.

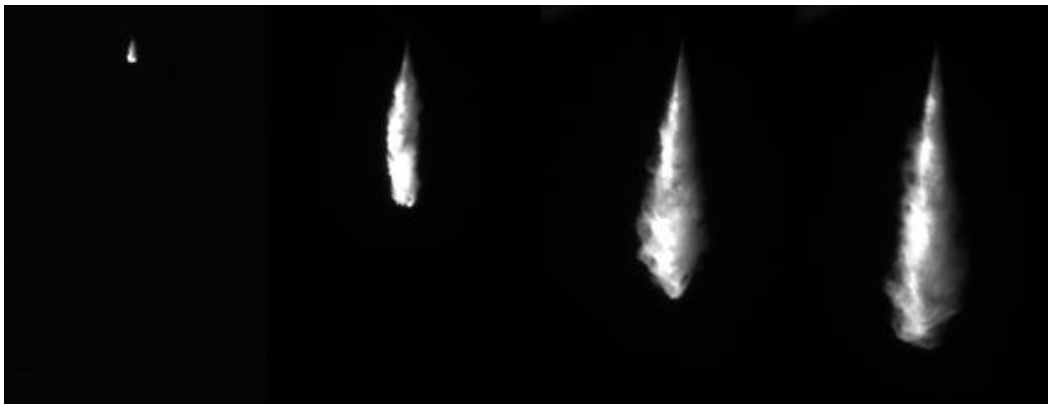

Figure 11: Sequence of injection events at 50, 250, 450, and 650 us ASOI

Figures 12 and 13 on the following two pages are an illustrative view of the shot-to-shot variation in penetration distance for injections into nitrogen at atmospheric pressure. Figure 11 shows the variability in measured penetration distance for the experimental setup using the engine control module system, while Figure 12 is representative of the manual injection system. The numbers on the right side of each graph represent the time after start of injection. Start of injection was determined from the onset of the first measurable signal above the background noise.

Figures 14 represents the coefficient of variance in penetration distance for each of the conditions listed in Table 2.

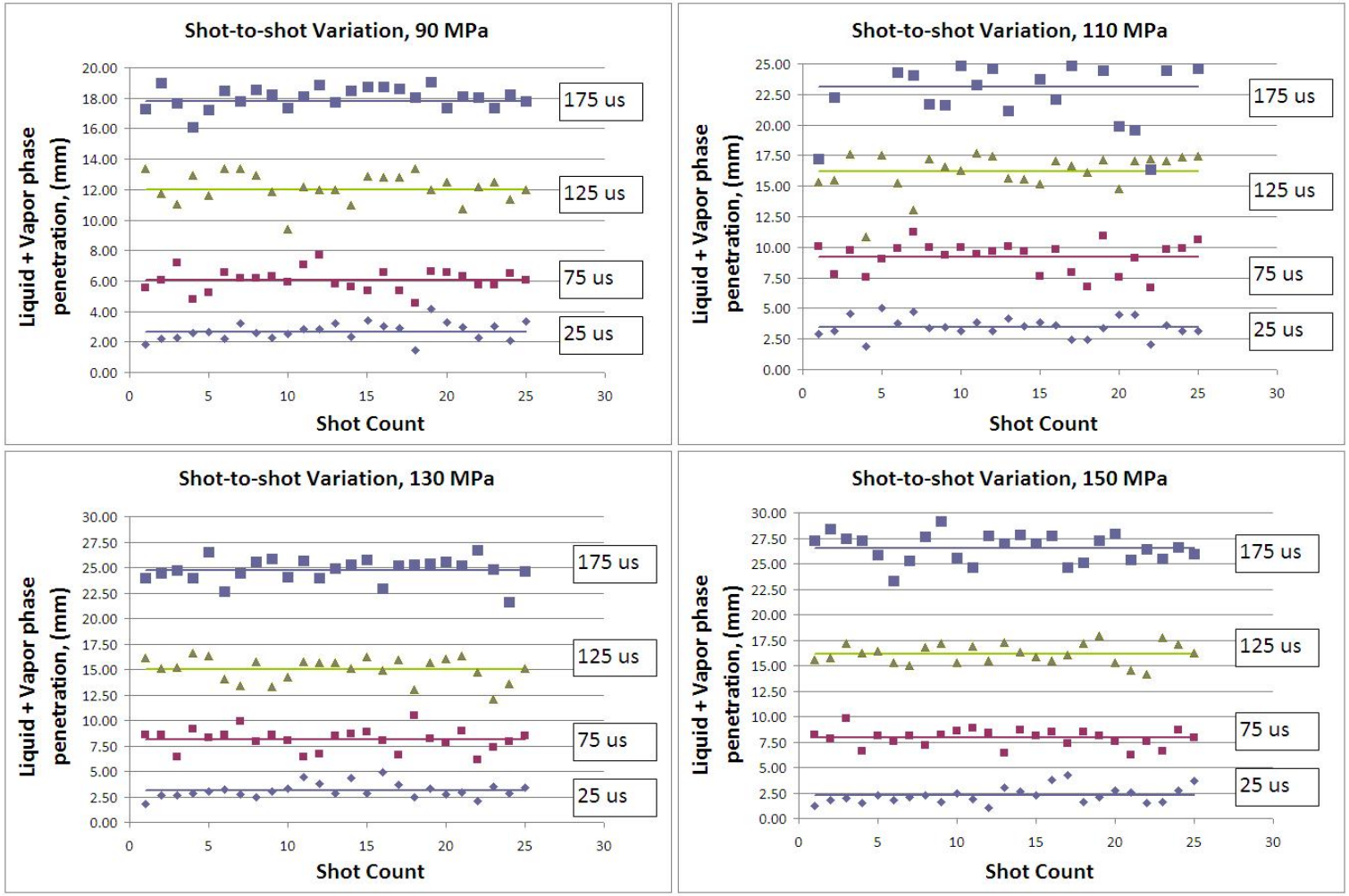

Figure 12: Shot-to-shot variation in penetration distance for the engine control module experimental setup

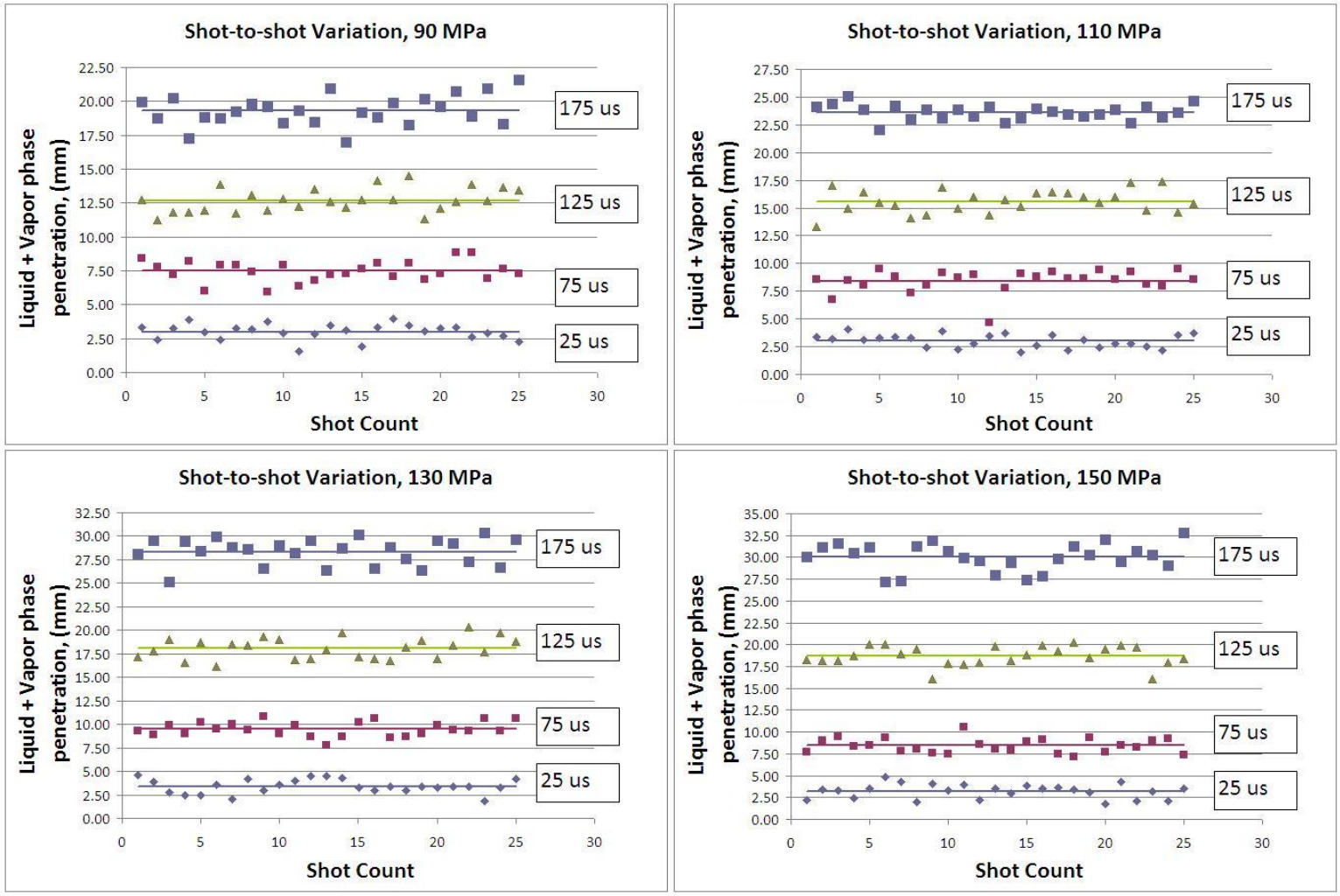

Figure 13: Shot-to-shot variation in penetration distance for the manual injection experimental setup

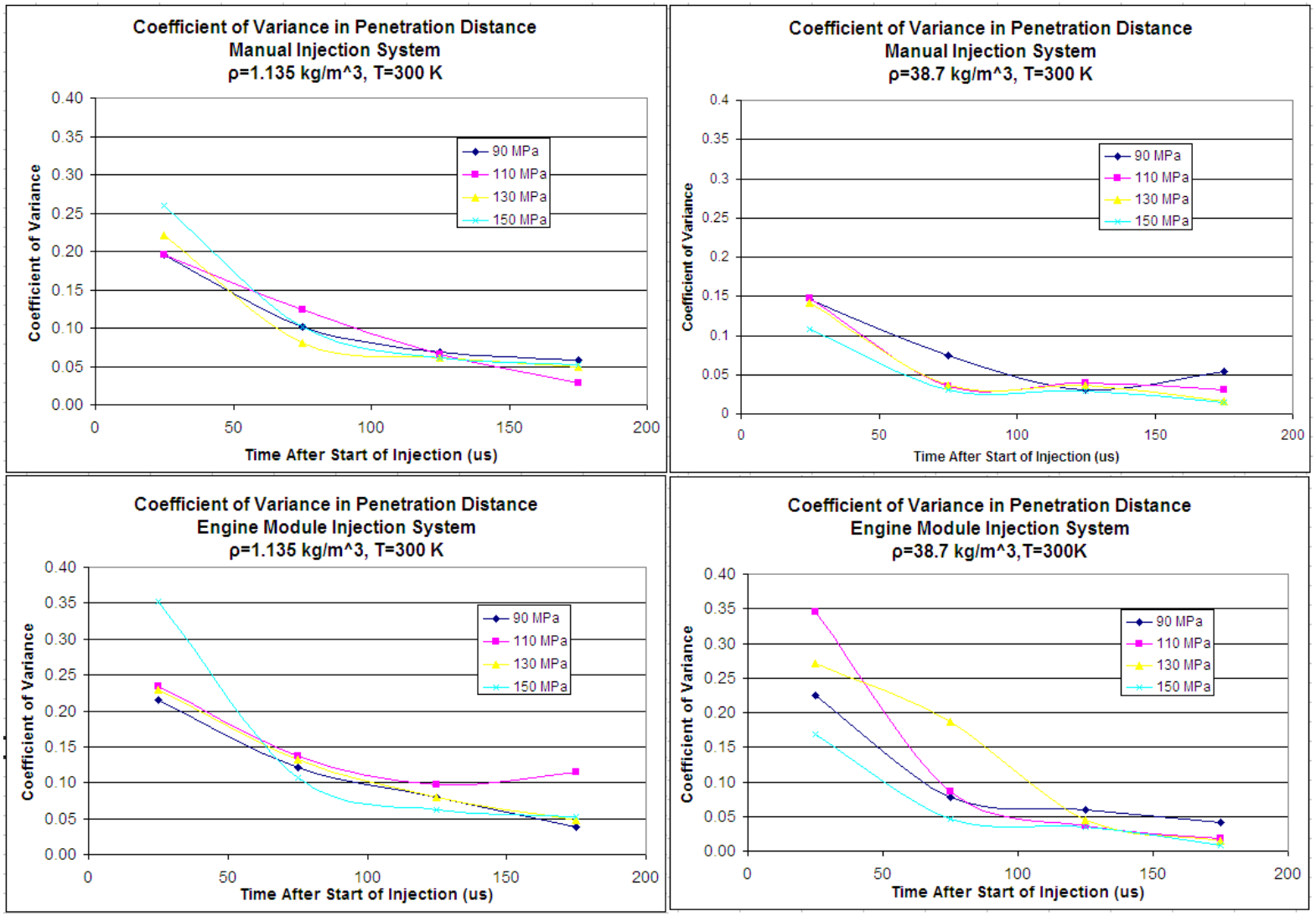

Figure 14: Coefficient of Variance in Penetration Distance for 90, 110, 130, and 150 MPa Fuel Injection Pressures, and Nitrogen Gas Densities of 1.135 and 38.7 kg/m^3.

Figures 12 and 13 show that the shot to shot penetration distance variation increases as the spray penetrates. Although this is the case, the ratio of penetration variation to total penetration distance decreases for the distances measured. This is evident in Figure 13 as negative slope values.

Figure 14 indicates that the manual injection method is marginally more consistent than the engine control module injection system. This effect could be misleading, however, because differences in fuel flow rate between the two injection systems could affect coefficient of variance values for the reason explained in the previous paragraph. In order to investigate this, the averaged penetration values for both injection systems are plotted in Figures 15 and 16 on the following two pages.

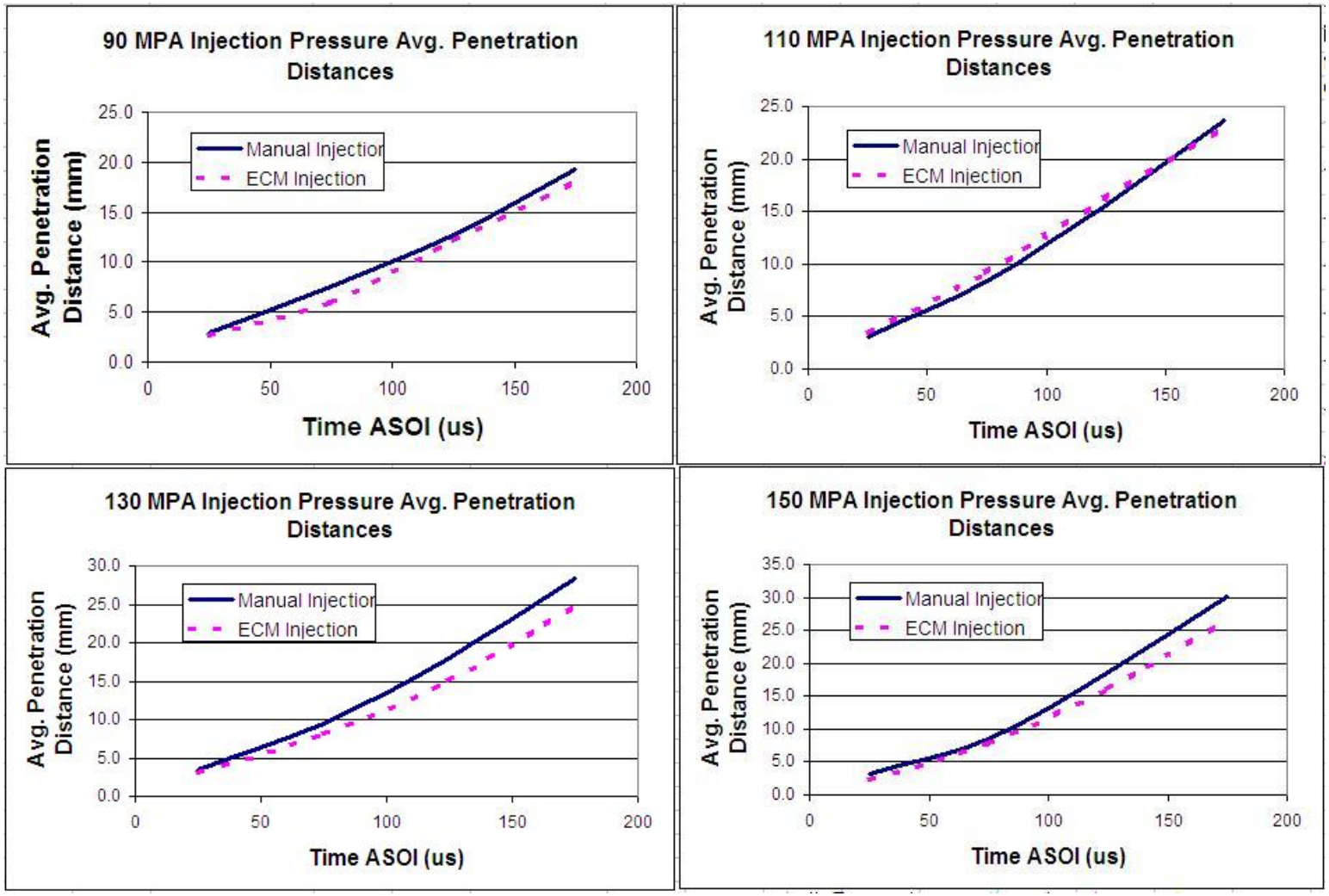

Figure 15: Average Penetration Distance Comparison between Manual and Engine Control Module Injection Methods into Nitrogen @ 101 kPa.

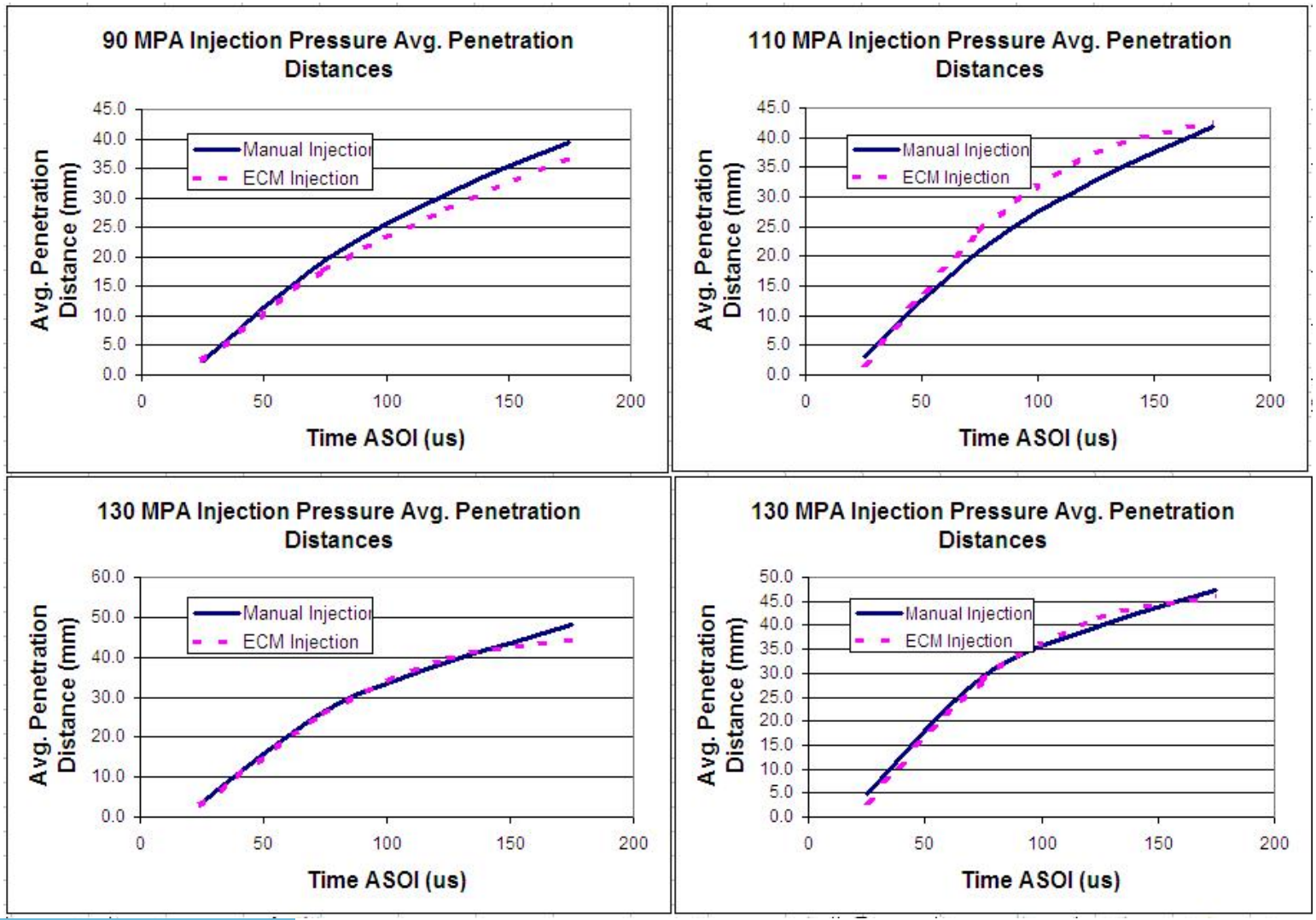

Figure 16: Average Penetration Distance Comparison between Manual and Engine Control Module Injection Methods into Nitrogen @ 101 kPa.

When injected into high pressure nitrogen at 3550 kPa, the diesel spray propagated much slower. This meant that for a given penetration distance, more fuel was present in the plume for injections into high gas pressures. The UV excitation source at 266nm was unable to pass through the spray for this case without significant attenuation occurring. The resulting effect can be seen in Figure 17, with the planar beam traveling from left to right.

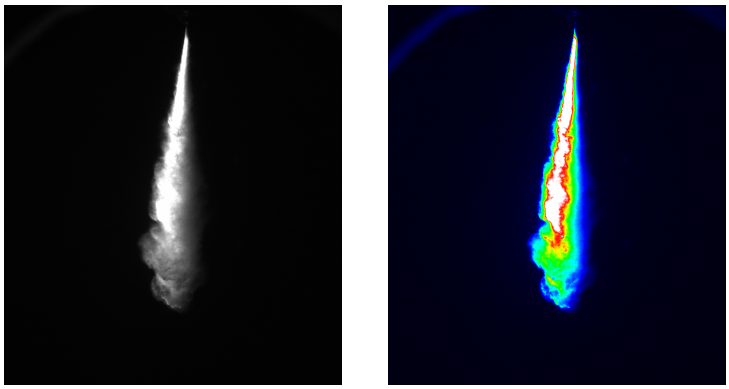

Figure 17: Illustration of Laser Attenuation for Injection into High Pressure Nitrogen.

Rather than correct for line of sight attenuation, planar images were experimented with for 355 nm excitation. As previously shown in Figure 3, the absorption of light in #2 fuel oil at 355 nm was much less than for 266 nm. Although this was expected to decrease the fluorescence signal, there was sufficiently more power available at 355 nm for PLIF studies. Since the attenuation was significantly less, the third harmonic at 355 nm was used for fluorescence studies thenceforth.

4.1.2 Fuel Oil #2 Photophysical Analysis

After selecting the 355nm beam for fluorescence studies, the photophysical response of #2 fuel oil was investigated. This was done by exciting a 30 ml sample of fuel oil and observing the response with a photodiode. This was done for three primary reasons.

First, a suitable filter needed to be selected to remove as much scatter from the spray signal as possible. Finding the wavelength at the onset of fluorescence signal was pivotal in determining the correct filter. The second reason for investigating photophysics was to select the proper optics for routing the fluorescence signal into the camera. Finally, the effect of temperature and pressure was investigated to determine if the excitation signal was significantly affected by the thermodynamic state of the fuel.

355 nm Spectral Response

The photophysical properties of diesel fuel oil #2 were investigated. First, the

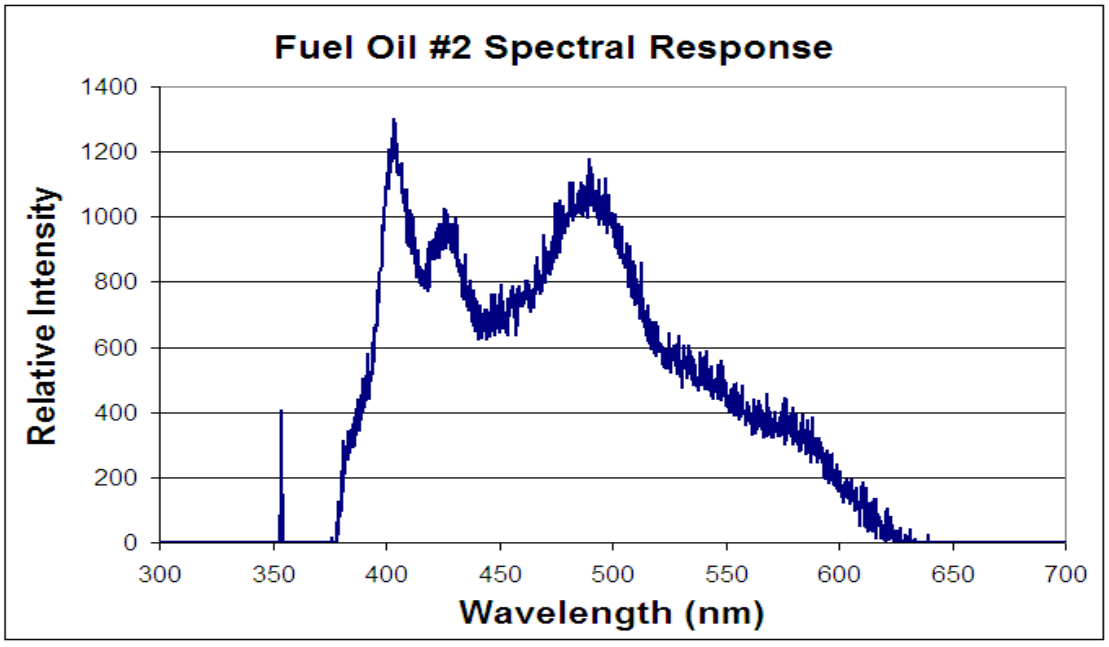

Figure 18: Unfiltered Spectral Response of Fuel Oil #2 with 355nm excitation.

fluorescence and phosphorescence spectrum of the diesel fuel used in the study was recorded for an excitation wavelength near 355 nm. The fluorescence and phosphorescence signals can be seen as peaks in Figure 18.

Because the signal in Figure 18 is unfiltered, some scattering was detected. This can be seen as a narrow peak at 355 nm. In order to reduce the effect of scattering during experimentation, a long-pass filter was installed with high attenuation below 400 nm. Figure 19 represents the spectral response seen by the imaging equipment with the filter in place. Although some attenuation can be observed between 400 and 450 nm, there was very little

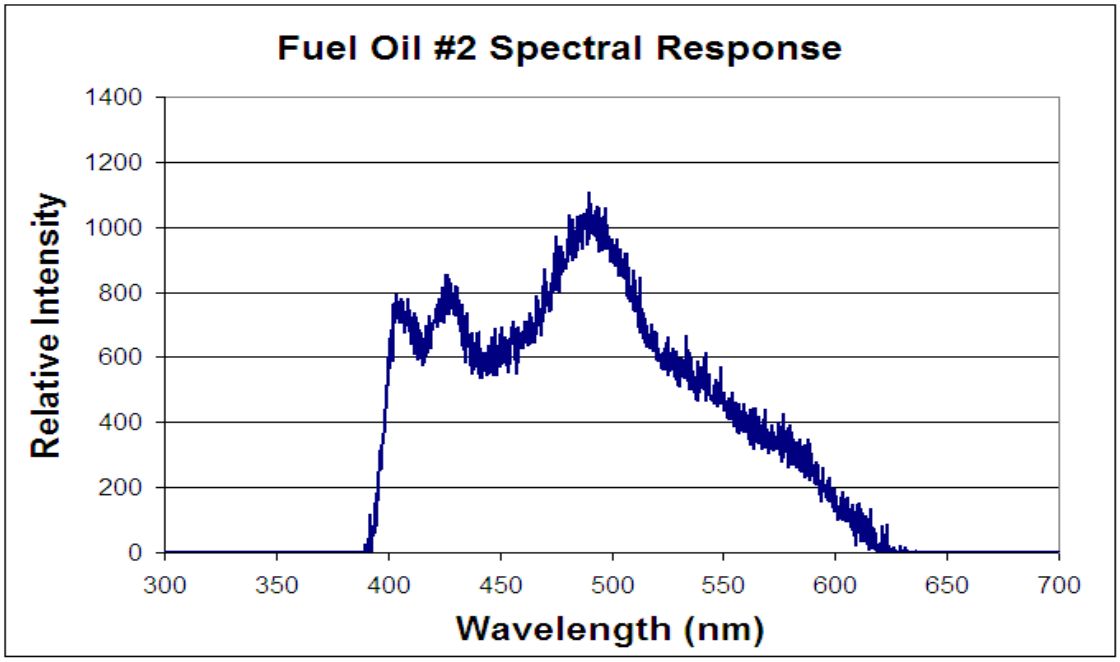

Figure 19: Spectral Response of Fuel Oil #2 with 355nm excitation and 400nm long-pass filter installed.

signal detected at 355 nm. As such, the filter was an effective tool for reducing signal due to scattering.

Fluorescent and Phosphorescent Lifetimes

The effect of temperature and pressure on fluorescent and phosphorescent lifetimes was investigated for 355 nm excitation of #2 Diesel Fuel. This was done to determine the photon emission duration of fuel molecules at various thermodynamic states. To do this, a photodiode was placed outside the aperture closest to the fuel injector of the constant volume vessel. A 400 nm long-pass filter was used to minimize scattering from the excitation source.

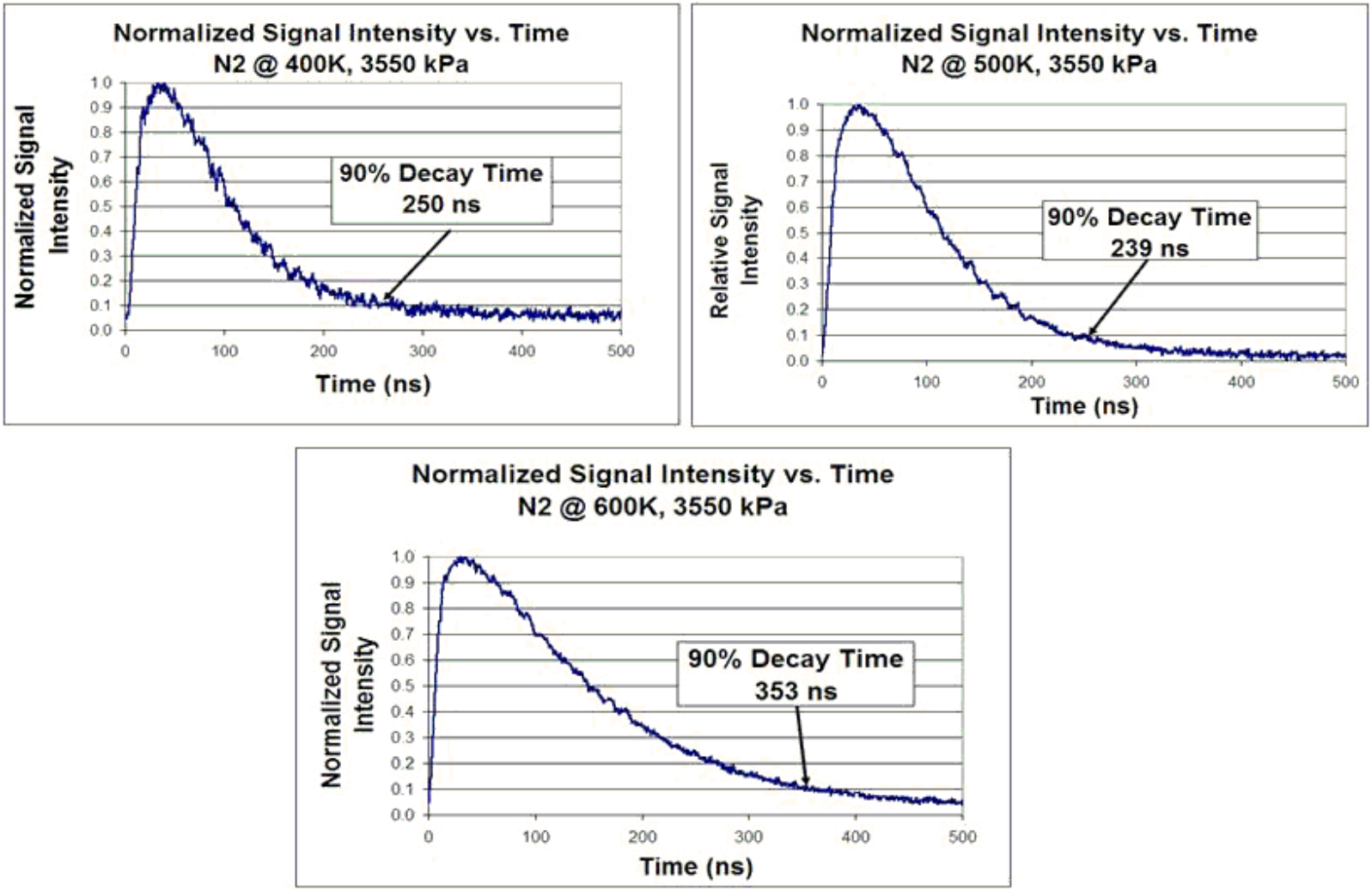

Figure 20: Elevated Temperature and Pressure Photophysical Response of Diesel Fuel #2 Vapor.

From Figure 20, the primary fluorescence signal can be seen to decay within 100-200 ns. Most of the signal following this period is likely phosphorescence, or photon emission from triplet states. Though photon emission occurs for approximately 1.5 us, the strongest part of the signal is visible in Figure 20. The 90 percent decay time of the longest lived signal from Figure 20 is approximately 350 ns. This led to very little image streaking for images.

Figure 21 shows a typical signal seen by the photodiode used to determine the temporal response of the fluorescence signal. This type of image was also used to ensure planar beam collimation and vertical alignment.

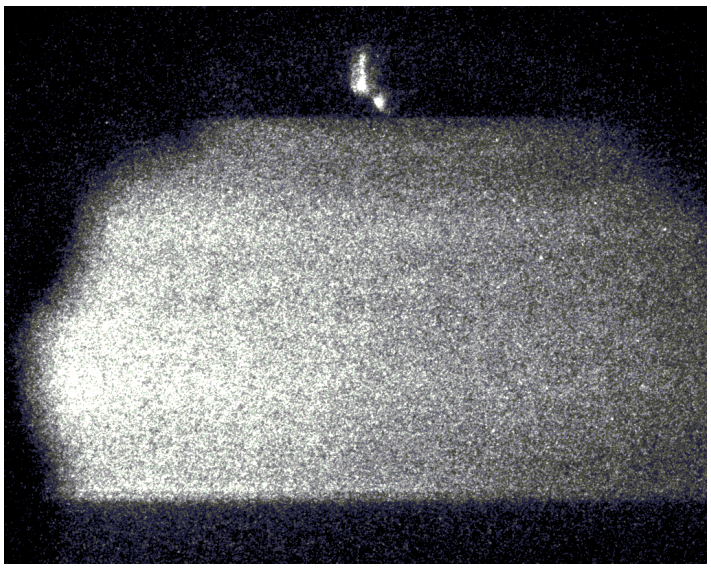

Figure 21: Fluorescence Signal of a Laser Sheet in Diesel Vapor.

4.2 High-Frequency Results

The results from high frequency PLIF are presented in the current section. Tests were conducted for 10 kHz and 20 kHz laser excitation frequencies. Figures 22 and 23 are raw image sequences for 10 kHz excitation into Nitrogen at 101 kPa and 3550 kPa, respectively.

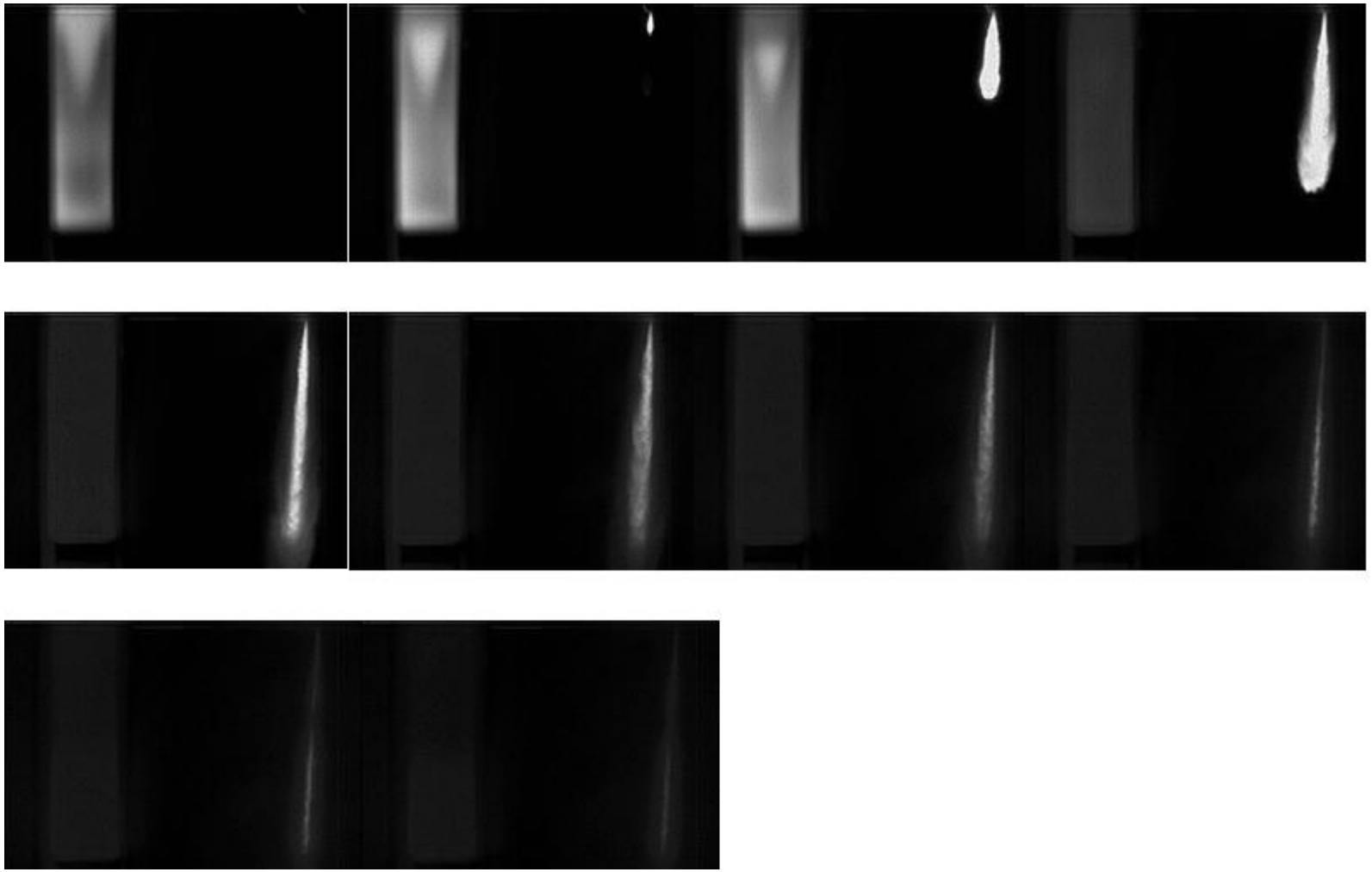

Figure 22: 90 MPa injection pressure into Nitrogen @ 101 kPa for laser excitation at 10 kHz.

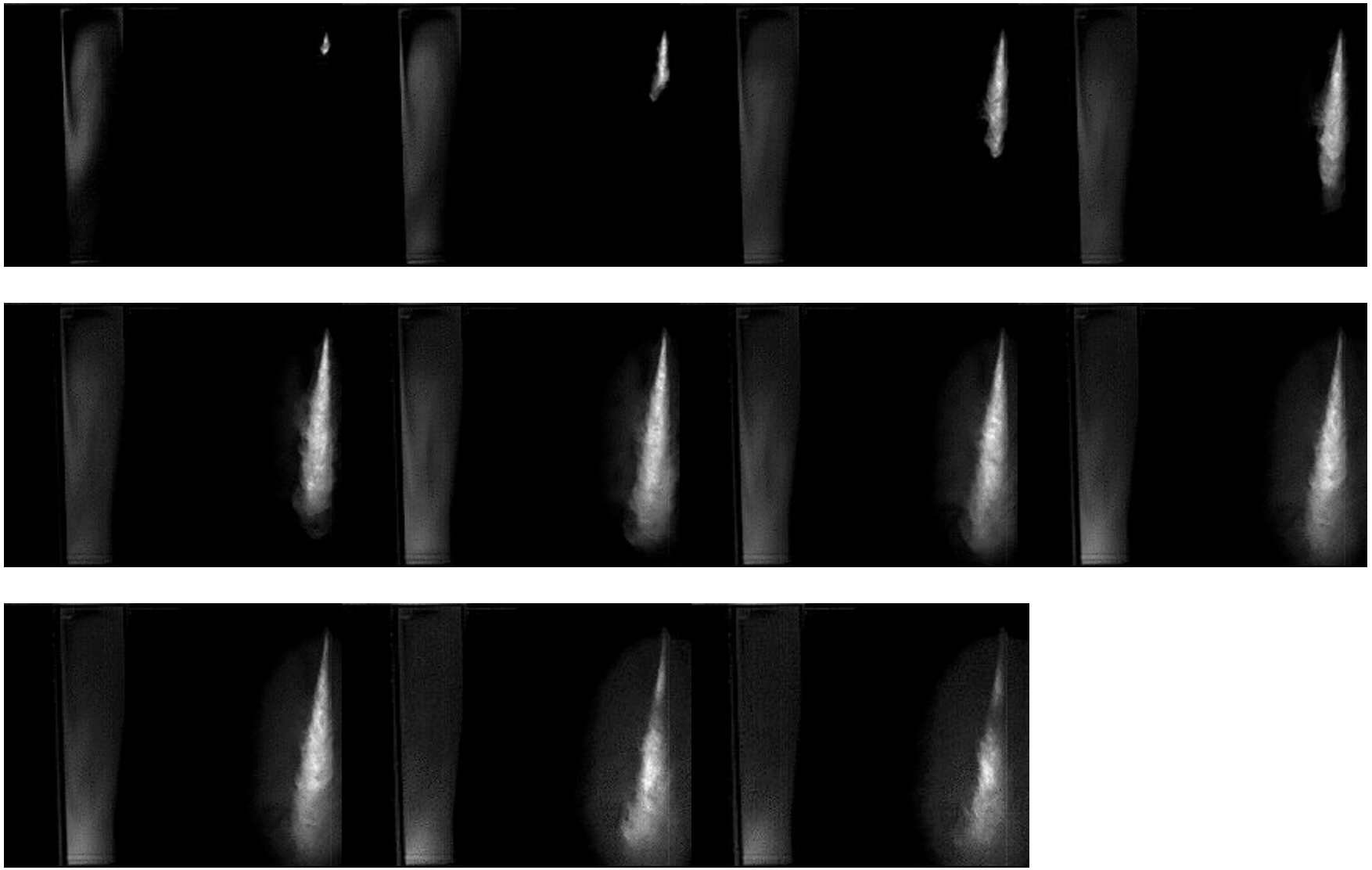

Figure 23: 100 MPa injection pressure into Nitrogen @ 3550 kPa for laser excitation at 10 kHz.

Figures 22 and 23 were achieved using laser sheets of approximately 45 mm in height and approximately 300 um in thickness at the injector tip. Energy output was near 35 mJ per pulse. The spatial and temporal distribution of pulse energy is evident in the calibration cell images on the left side of the spray images. For all high frequency studies, 355 nm excitation was used. The calibration fluid used for these studies was a laser dye known as LD489 [45]. The laser sheet was passed through the fluid-filled calibration cell prior to the spray. To utilize the dynamic intensity range camera array, the concentration of LD489 calibration fluid was varied to find the optimal setup. To do this, LD489 was diluted with Methanol in varying concentrations. Methanol was used as the solvent because it did not appreciably absorb light at 355 nm. The optimal setup was realized when the both the calibration fluid and spray signal intensities were near each other. This allowed the abundance of signal to be attenuated to the optimal setting.

Although the raw images from Figures 22 and 23 have sufficient signal energy, it was necessary to correct for spatial variations in the laser beam. Figure 24 illustrates the relative variation in pulse energy for eight laser sheets. The first pixel count of Figure 24 corresponds to the bottom of the calibration cell seen in Figures 22 and 23. To adjust the images, a correction factor was calculated by first averaging the background subtracted calibration cell intensity values in the horizontal direction for each image frame. The raw spray image values were then divided by the averaged calibration cell intensity values.

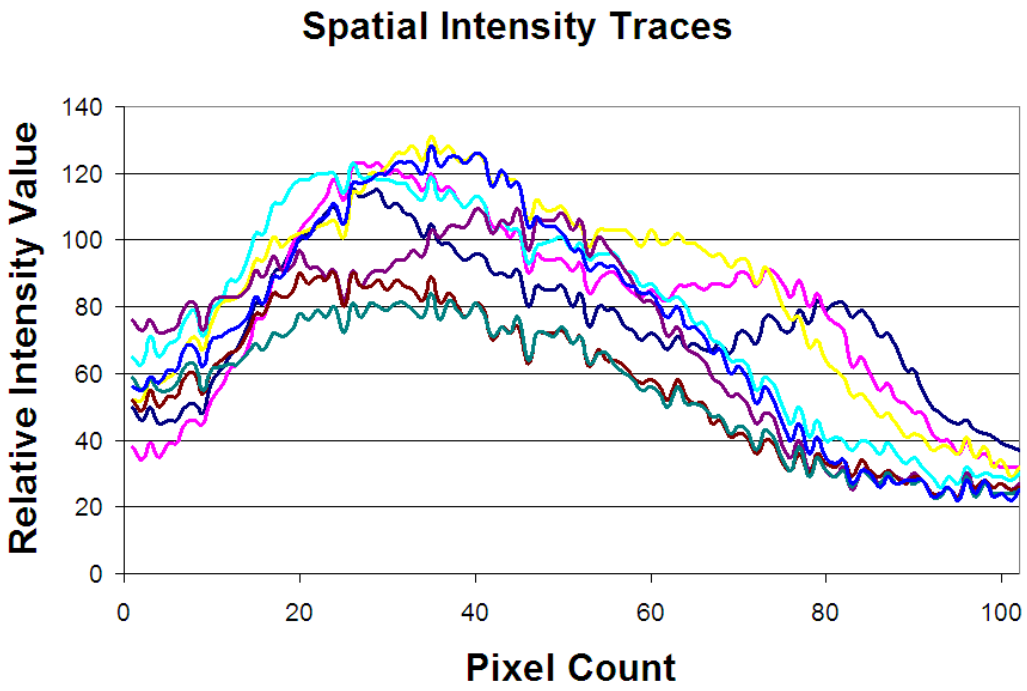

Figure 24: Eight intensity traces from the calibration cell signal of a single injection event

Figure 25 illustrates the methodology used for image processing. The location of the injector orifice was determined in the image by locating the first vertical location where the image intensity was greater than five times the averaged background value. For example, the location of the injector orifice in Figure 24 can be seen as a steep rise in intensity values.

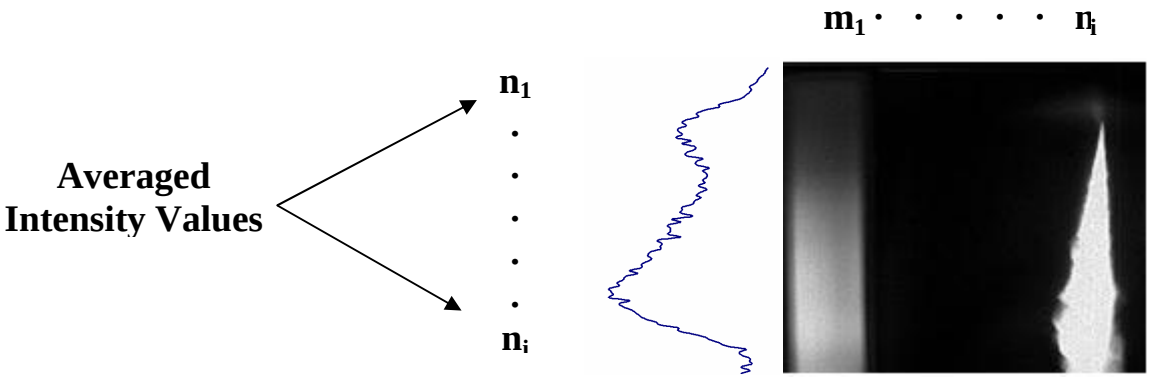

Figure 25: Illustration of calibration cell averaged intensity values.

For an image matrix of [I] of n x m dimensions, a given row "n_i" of "m" values was normalized by n_i. In summary, the images were processed by the following method:

Corrected Image Pixel n_i=(Raw Image – (Background+Scattering)) / Correction Factor n_i

Since the absorption of light in fuel was relatively low for 355 nm, the attenuation was not corrected for. Figures 26, 27, and 28 show the corrected image sequences for 100, 125, and 150 MPa injection pressures, respectively.

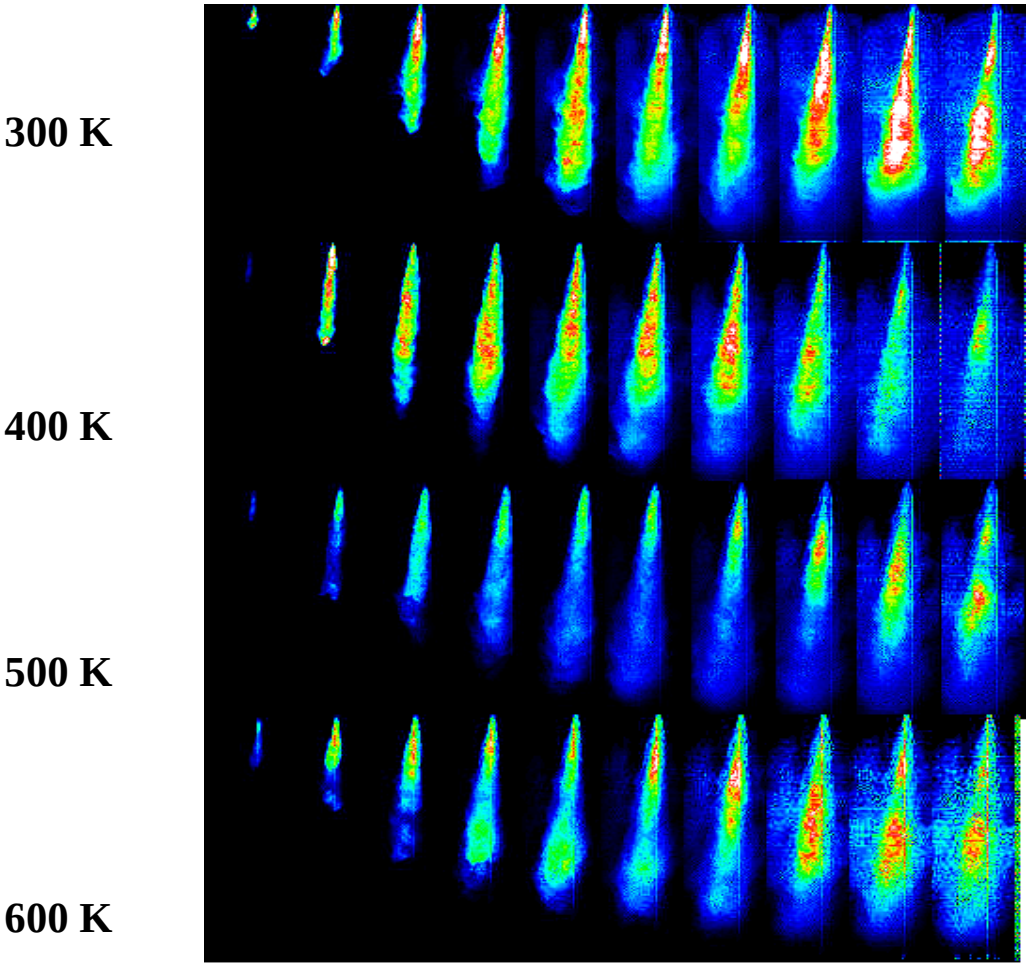

Figure 26: 100 MPa injection sequence into N2 @ 3550 kPa

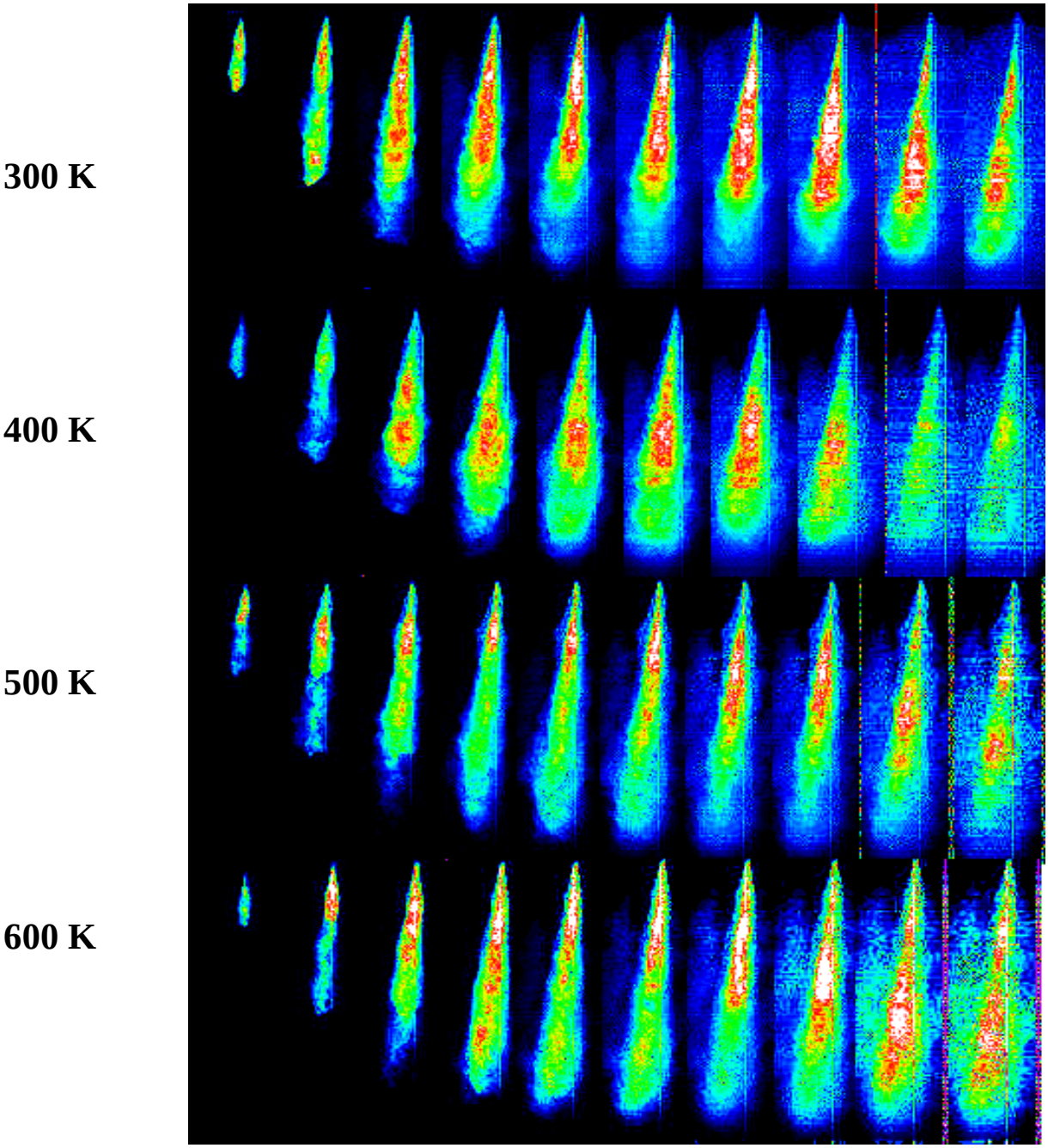

Figure 27: 125 MPa injection sequence into N2 @ 3550 kPa

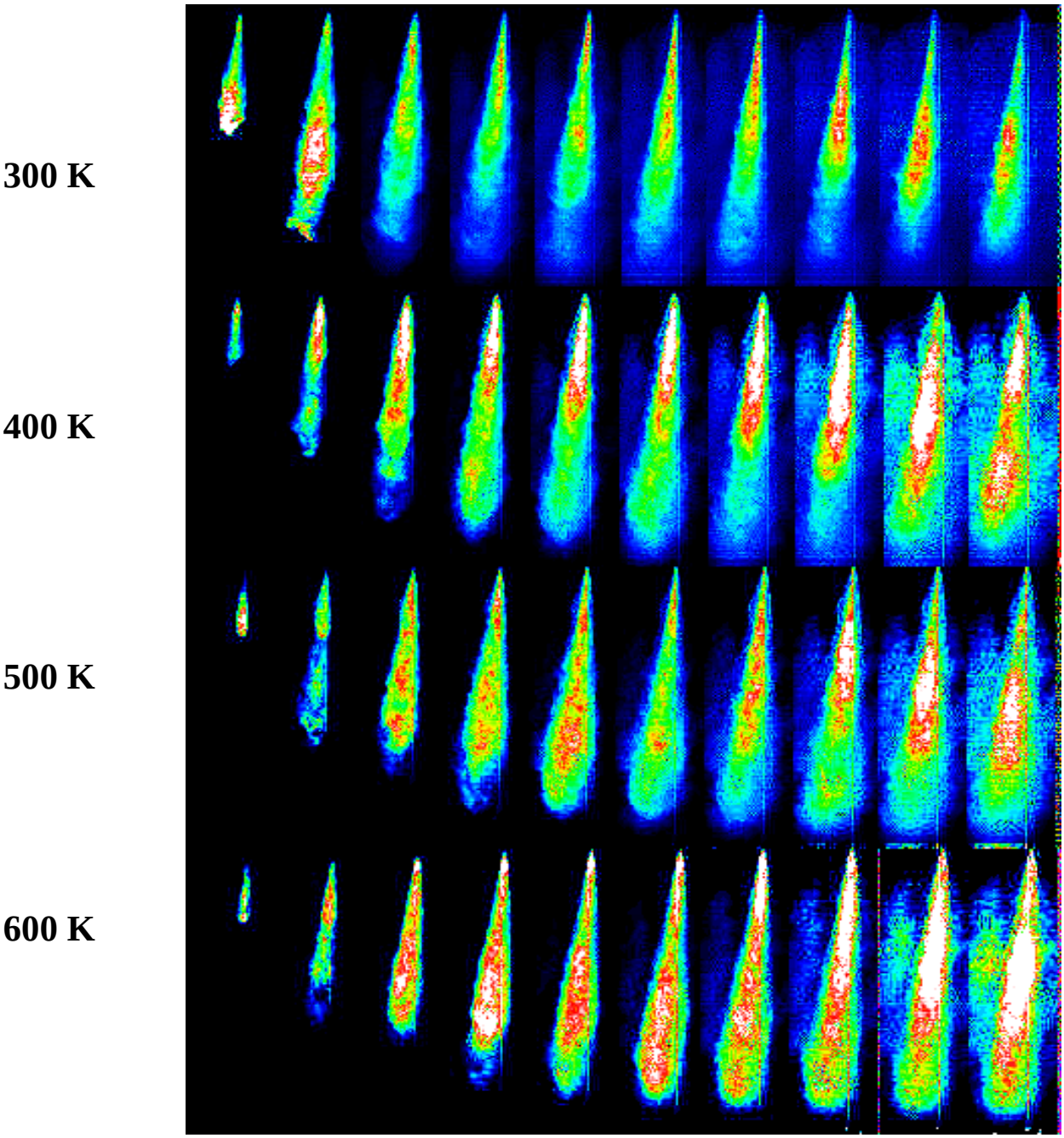

Figure 28: 150 MPa injection sequence into N2 @ 3550 kPa

Since the images of Figures 26-28 were acquired at 10 kHz, the spacing between images is approximately 100 us. The continuous dense liquid core of the spray can clearly be seen in the first several images of each sequence. Images from early in the injection show that initially the tip of the spray plume is very dense prior to breaking up. Once the injector is fully open, however, the spray appears to reach a steady liquid phase distribution. As the laser pulses become weaker later in the sequence, it becomes increasingly difficult to resolve the concentration distribution.

After imaging the spray at 10 kHz, it was desired to investigate the spray with greater temporal resolution. This was achieved using excitation pulses at 20 kHz. As such, Figure 29 is an sequence of raw images from an injection event at 90 MPa injection pressure into nitrogen at 3550 kPa pressure. The spatial laser variation is evident in the calibration cell at the left side of each spray image.

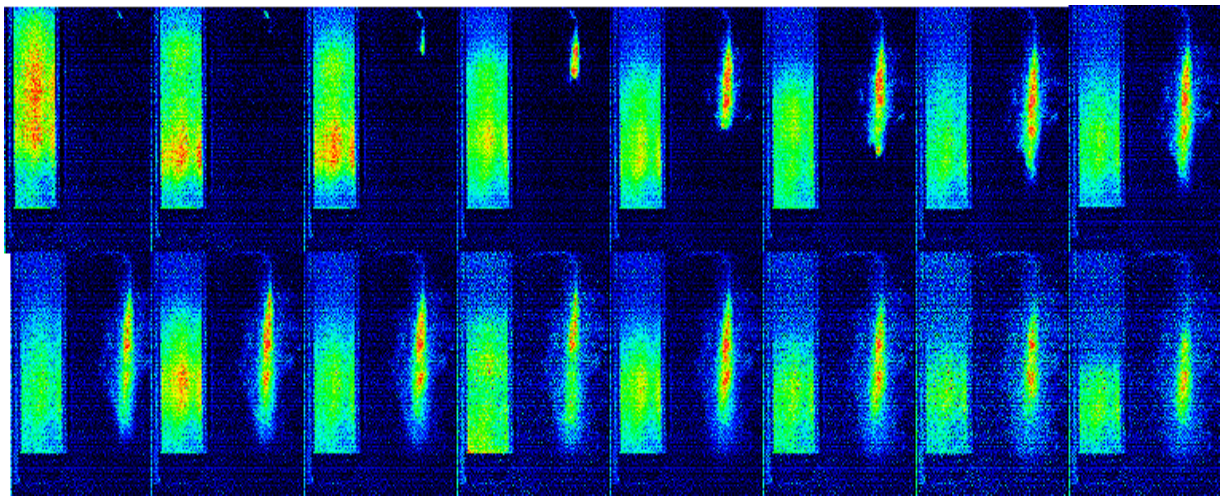

Figure 29: Raw Image Sequence at 20 kHz

Figure 30 shows the normalized images from Figure 29. The correction was performed using the same method as for the 10 kHz case.

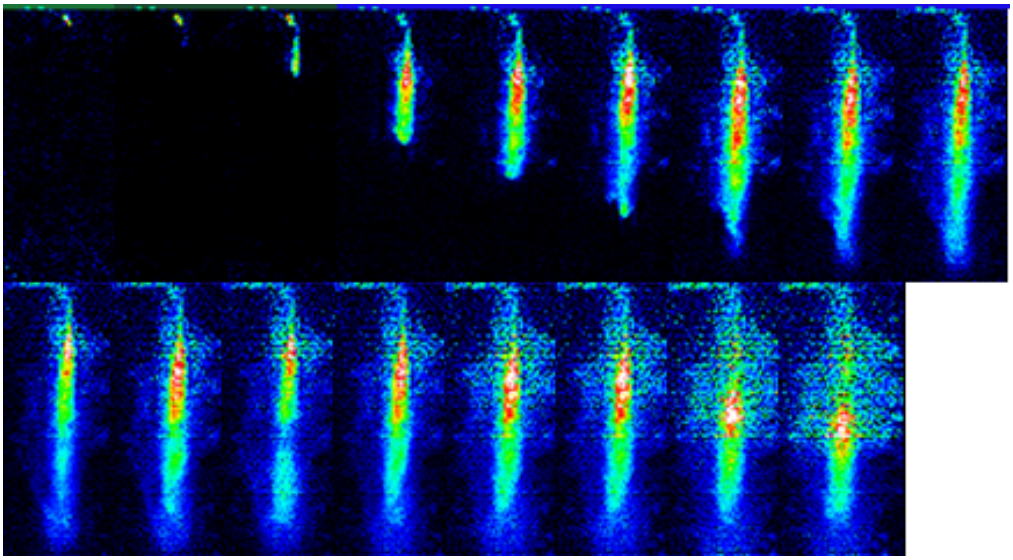

Figure 30: Image Sequence at 20 kHz

The corrected spray images of Figure 30 show the high concentration areas of the spray near the injector tip early in the injection. As the spray entered the chamber, the first droplets were observed to decelerate significantly. The fuel behind this region, however, maintained its initial velocity and propagated through the deceleration region at high velocity until losing momentum to the surrounding gas. This type of event was observed to occur two to three times per injection event for the distances examined. This illustrates that the tip velocity of the spray can either increase or decrease at a given time after start of injection.

As the images progress in time, there is observed to be an abundance of signal around the periphery of the spray. This was likely due to signal scattering and reflection from the opposite side of the constant volume vessel. Since the camera aperture open time was 50 us, there was significant integration time for extra light to populate the CCD array.

In addition to the normalized images from Figure 30, seven additional injection events were acquired to investigate the shot-to-shot penetration variation. Figure 31 shows penetration curves for eight injection events.

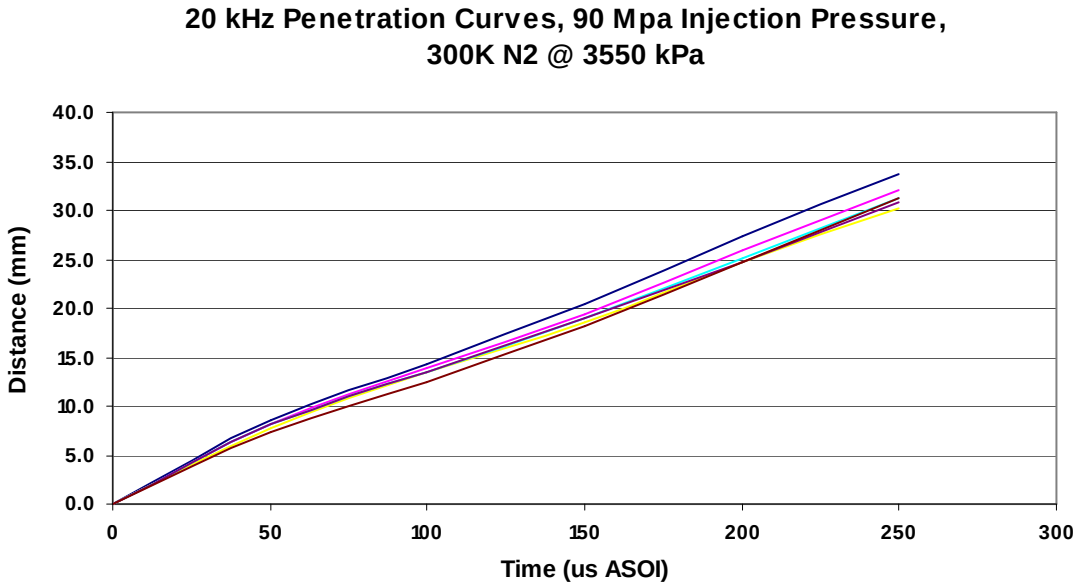

Figure 31: Diesel spray penetration curves

As can be seen in Figure 31, the overall penetration distance tends to vary increasingly the further it propagates. Shot-to-shot spray propagation variability could be a contributor to instability in soot and NOx production in diesel flames. This effect could be determined by investigating diesel diffusion flames at high frequency.

CHAPTER 5. SUMMARY AND CONCLUSIONS

A constant volume combustion vessel was refurbished for use at Iowa State University in collaboration with John Deere. The vessel contains four points of optical access which are used to image diesel injection events. Due to the high velocity of typical diesel sprays, images were acquired using planar laser-induced fluorescence. Preliminary studies were performed to determine shot-to-shot variations in spray penetration.

Following preliminary studies, a high-frequency planar laser induced fluorescence method was implemented to image individual diesel fuel injection events. Laser excitation was provided using the output of a pulse-burst laser system. The beam was formed into a sheet of approximately In concert with the pulse burst diagnostic system, a calibration system was developed for the shot-to-shot normalization of individual sprays. This was accomplished by filling a calibration cell with a mixture of methanol and LD489 laser dye. The mixture concentration was adjusted as necessary to optimize the signal intensities of the calibration fluid and spray.

Spray penetration was resolved for fuel injections into atmospheric (1.135 kg/m^3) and high density (38 kg/m^3) nitrogen for a variety of gas temperatures and injection pressures. The results indicate that the minimum excitation frequency for temporally resolving diesel injection events is approximately 10-20 kHz, depending on the gas pressure.

The raw images were corrected for spatial variations in laser energy to yield images detailing the liquid phase concentration distribution of diesel sprays.

Using a similar technique, high-frequency, quantitative planar images of molecules such as OH, NO, and CH could be acquired for a single injection event. This would allow temporally resolved tracking of species concentrations. The intent of such a study could be

to validate CFD models or test diesel engine components. The system could also be well suited to optical engine tests, which could yield individual cycle species distribution and evolution.

REFERENCES

[1] www.epa.gov

[2] Eckbreth, Alan C. Laser Diagnostics for Combustion Temperature and Species. Dallas: Taylor & Francis, 1996.

[3] Carling, Robert W. and Gurpreet Singh. “Overview of Engine Combustion Research at Sandia National Laboratories.” SAE Paper 1999-01-2246 (1999).

[4] Schulz, Christof, and Volker Sick. “Tracer-LIF diagnostics: quantitative measurement of fuel concentration, temperature and fuel/air ratio in practical combustion systems.” Prog. Energy Combust. Sci Vol. 31 (2005): 75-121.

[5] "Imaging of advanced low-temperature diesel combustion." CRF News: Science and Technology for Energy and National Security 27 (2005): 2-2. <http://public.ca.sandia.gov/crf/newspubs/CRFnews/index.php>.

[6] Yule, A.J., and S.M. Aval. "Cyclic Variations of Diesel Sprays." FUEL Vol. 68 (1989): 1558-564.

[7] Schaller, Johannes K., and Christo G. Stojanoff. "Holographic Investigations of a Diesel Jet Injected into a High-Pressure Test Chamber." (1996).

[8] Kennaird, D.A., C. Crua, J. Lacoste, M.R. Heikal, and M.R. Gold. "In-Cylinder Penetration and Break-Up of Diesel Sprays Using a Common-Rail Injection System." SAE Paper 2002-01-1626 (2002).

[9] Higgins, B.S., C.J. Mueller, and Dennis L. Siebers. "Measurements of Fuel Effects on Liquid-Phase Penetration in DI Sprays." SAE Paper 1999-01-0519 (1999).

[10] Baik, S., J.P. Blanchard, and M.L. Corradini. "Development of Micro-Diesel Inejctor Nozzles via Microelectromechanical Systems Technology and Effects on Spray Characteristics." Journal for Engineering of Gas Turbines and Power 125 (2003).

[11] Cronhjort, Andreas, and Fredrik Wahlin. “Segmentation algorithm for diesel spray image analysis.” Applied Optics Vol. 43 (2004): 5971-5980.

[12] Wang, T.C., J.S. Han, X.B. Xie, M.C. Lai, N.A. Henein, E. Schwarz, and W. Bryzik. "Parametric Characterization of High-Pressure Diesel Fuel Injection Systems." Transactions of the ASME 125 (2003).

[13] Delacourt, E., B. Desmet, and B. Besson. "Characterization of very high pressure diesel sprays using digital imaging techniques." FUEL 84 (2005): 859-67.

[14] Wu, Zhijun, Zhu, Zhiyong, and Huang, Zhen. “An experimental study on the spray structure of oxygenated fuel using laser-based visualization and particle image velocimetry.” FUEL Vol. 85 (2006): 1458-1464.

[15] Zhang, Yu-yin, Takuo Yoshizaki, and Keiya Nishida. "Imaging of droplets and vapor distributions in a Diesel fuel spray by means of a laser absorption-scattering technique." Applied Optics 39 (2000): 6221-229.

[16] Wissel, S., Hoffmann, T., Hottenbach, P., Koss, H.-J., Pauls, C., and Grunefeld, G. “Droplet Velocity Measurements in Direct-Injection Diesel Sprays Under High-Pressure and High-Temperature Conditions by Laser Flow Tagging.” SAE Paper 2008-08-0944 (2008).

[17] Linne, M.A., and T.E. Parker. Ballistic Imaging in the Primary Breakup Region of Diesel Injector Sprays. Engineering Division, Colorado School of Mines. 2006.

[18] Linne, Mark, Megan Paciaroni, Tyler Hall, and Terry Parker. "Ballistic imaging of the near field in a diesel spray." Experiments in Fluids 41 (2006): 836-46.

[19] MacPhee, Andrew G., Mark W. Tate, Christopher F. Powell, Yon Yue, Matthew J. Renzi, Alper Ercan, Suresh Narayanan, Ernest Fontes, Jochen Walther, Johannes Schaller, Sol M. Gruner, and Jin Wang. "X-ray Imaging of Shock Waves Generated by High-Pressure Fuel Sprays." SCIENCE 295 (2002): 1261-263.

[20] Yue, Yong, Christopher F. Powell, Ramesh Poola, Jin Wang, and Johannes K. Schaller. "Quantitative measurement of diesel fuel spray characteristics in the near-nozzle region by using X-ray absorption." Atomization and Sprays 11 (2001): 1-20.

[21] Bougie, B., Tulej, M., Dreier, T., Dam, N.J., Ter Meulen, J.J., and Gerber, T. “Optical diagnostics of diesel spray injections and combustion in a high-pressure high-temperature cell.” Applied Physics B: Lasers and Optics 80 (2005): 1039-1045.

[22] Mirza, M.R., Baluch, A.H., and Tahir, Z.R. “Structure of Non-Evaporating Diesel Sprays.” Pak. J. Engg. & Appl. Sci. Vol. 2 (2008).

[23] Morgan, R., Wray, J., Kennaird, D.A., Crua, C., and M.R. Heikal. “The Influence of Injector Parameters on the Formation and Break-Up of a Diesel Spray.” SAE Paper 2001-01-0529 (2001).

[24] Ochoterena, R., Larsson, M., Andersson, S., and Denbratt, I. “Optical Studies of Spray Development and Combustion Characterization of Oxygenated and Fischer-Tropsch Fuels.” SAE Paper 2008-01-1393 (2008).

[25] Desantes, J.M., Payri, R., Garcia, J.M., and Salvador, F.J. “A contribution to the understanding of isothermal diesel spray dynamics.” FUEL Vol. 86 (2007): 1039-1101.

[26] Hillamo, Harri, Kaario, Ossi, and Larmi, Martti. “Particle Image Velocity Measurements of a Diesel Spray.” SAE Paper 2008-01-0942 (2008).

[27] Gaydon, A.G., and H.G. Wolfhard. Flames: Their structure, radiation and temperature. 4th ed. New York: Chapman and Hall, 1979.

[28] Pickett, Lyle M., and Dennis L. Siebers. ASME ICE Division Fall Technical Conference, 2001, Chicago. Orifice Diameter Effects on Diesel Fuel Jet Flame Structure.

[29] Pickett, Lyle M., and Siebers, Dennis L. “An Investigation of Diesel Soot Formation Processes using Micro Orifices.” Proceedings of the Combustion Institute 30 (2002).

[30] Ito, Takayuki, Takaaki Kitamura, Masato Ueda, Takeo Matsumoto, Jiro Senda, and Hajime Fujimoto. "Effects of Flame Lift-Off and Flame Temperature on Soot Formation in Oxygenated Fuel Sprays." SAE Paper 2003-01-0073 (2003).

[31] Pickett, Lyle M., and Siebers, Dennis L. "Non-Sooting, Low Flame Temperature Mixing-Controlled DI Diesel Combustion." SAE Paper 2004-01-1399 (2004).

[32] Pickett, Lyle M., and Dennis L. Siebers. "Soot in diesel fuel jets: effects of ambient temperature, ambient density, and injection pressure." Combustion and Flame (2004): 114-135.

[33] Pickett, Lyle M., Dennis L. Siebers, and C.A. Idicheria. "Relationship between ignition processes and the lift-off length of diesel fuel jets." SAE Paper 2005-01-3843 (2005).

[34] Pickett, Lyle. “Low flame temperature limits for mixing-controlled Diesel combustion.” Proceedings of the Combustion Institute 30 (2005).

[35] Musculus, Mark P.B., and Pickett, Lyle M. “Diagnostic considerations for optical laser-extinction measurements of soot in high-pressure transient combustion environments.” Combustion and Flame 141 (2005): 371-391.

[36] Pickett, Lyle M., and J. Javier Lopez. "Jet-Wall Interaction Effects on Diesel Combustion and Soot Formation." SAE Paper 2005-01-0921 (2005).

[37] Pickett, Lyle M. and Idicheria, Cherian A., “Soot Formation in Diesel Combustion under High-EGR Conditions.” SAE Paper 2005-01-3834 (2005).

[38] Svensson, Kenth I. Effects of Fuel Molecular Structure and Composition on Soot Formation in Direct-Injection Spray Flames. Diss. Brigham Young University, 2005.

[39] Tree, Dale R., and Kenth I. Svensson. “Soot processes in compression ignition engines.” Prog. Energy Combust. Sci Vol. 33 (2007): 272-309.

[40] Zhao, H., and N. Ladommatos. "Optical Diagnostics for Soot and Temperature Measurement in Diesel Engines." Prog. Energy Combust. Sci. Vol. 24 (1998): 221-55.

[41] Borman, Gary L., and Kenneth W. Ragland. Combustion Engineering. New York: McGraw-Hill Higher Education, 2004.

[42] Hoffmann, T., Hottenbach, P., Koss, H.-J., Pauls, C., and Grunefeld, G. “Investigation of Mixture Formation in Diesel Sprays under Quiescent Conditions using Raman, Mie, and LIF Diagnostics.” SAE Paper 2008-01-0945 (2008).

[43] Pastor, Jose V., Jose J. Lopez, J. Enrique Julia, and Jesus V. Benajes. "Planar Laser-Induced Fluorescence fuel concentration measurements in isothermal Diesel sprays." Optics Express 10 (2002): 309-23.

[44] Greenhalgh, D.A. "Laser imaging of fuel injection systems and combustors." Proc. Instn. Mech. Engrs. 214 (2000): 367-76.

[45] http://www.oxfordlasers.com

[46] Stojkovic, Boris D., Fansler, Todd D., Drake, Michael C., and Sick, Volker. "High-speed imaging of OH* and soot temperature and concentration in a stratified-charge direct-injection gasoline engine." Proceedings of the Combustion Institute 30 (2005): 2657-2665.

[47] J. Hult, A. Harvey, and C. F. Kaminski, "Combined high repetition-rate OH PLIF and stereoscopic PIV for studies of turbulence/chemistry interactions," in *Laser Applications to Chemical and Environmental Analysis*, Technical Digest (Optical Society of America, 2003), paper MF3.

[48] Hult, Johan, Mattias Richter, Jenny Nygren, Marcus Alden, Anders Hultqvist, Magnus Christensen, and Bengt Johansson. "Application of a high-repetition-rate laser diagnostic system for single-cycle-resolved imaging in internal combustion engines." Applied Optics 41 (2002): 5002-5014.

[49] Hultqvist, Anders, Magnus Christensen, Bengt Johansson, Mattias Richter, Jenny Nygren, Johan Hult, and Marcus Alden. "The HCCI Combustion Process in a Single Cycle-High-Speed Fuel Tracer LIF and Chemiluminescence Imaging." SAE Paper 2002-01-0424 (2002).

[50] Miller, Joseph, Slipchenko, Mikhail, Meyer, Terrence, Jiang, Naibo, Lempert, Walter, and Gord, James. Ultrahigh-frame-rate OH fluorescence imaging in turbulent flames using a burst-mode optical parametric oscillator. Submitted for publication in Optics Letters, 2008.

[51] Jiang, Naibo, Lempert, Walter, Switzer, Gary, Meyer, Terrence, and Gord, James. "Narrow-linewidth megahertz-repetition-rate optical parametric oscillator for high-speed flow and combustion diagnostics." Applied Optics 47 (2008): 64-71.

[52] Chattopadhyay, Somnath. Pressure Vessels: Design and Practice. New York: CRC Press, 2005.

APPENDIX: ADDITIONAL MATERIAL

Structural Analysis

In this section, a chronological procession of the structural analysis is presented. This analysis is intended to serve as a guideline for determining the allowable operating conditions. In order to determine operational limits, classical calculations were first performed. According to Chattopadhyay [52], the maximum stress seen in an internally pressurized cylindrical pressure vessel with a circular hole is

$$\sigma_{t,\max} = \frac{\sigma}{4}\left(4 + \frac{3a^2}{r^2} + \frac{3a^4}{r^4}\right),$$

Where, *a* is the hole radius, *r* is interior radius of the pressure vessel, and σ corresponds to the theoretical hoop stress seen in the pressure vessel as specified by σ_t in the following equation:

$$\sigma_t = \frac{P}{m^2 - 1}\left(1 + \frac{r_0^2}{r^2}\right)$$

The hoop stress is determined as a function of the internal vessel pressure *P*, the ratio of the outer radius to the inner radius *m*, and the outer and the dimensions of the inner radii r_o and *r*, respectively.

The next step of the analysis was to develop a finite element model for the pressure vessel. This was done using the Cosmos Works FEA package within Solid Works software. In order to validate the results of the classical calculations, a number of simulations were run. The purpose of these simulations was to determine the approximate magnitude of the maximum stress experienced by the pressure vessel. The location of maximum stress indicated by FEA was also used as a guideline to ensure results were reasonable.

Figure A2 contains the results from both the classical calculations and FEA. As can be seen, there is reasonable agreement between the classical calculations and FEA results. The most likely source of discrepancy between the values shown in this case is the assumed

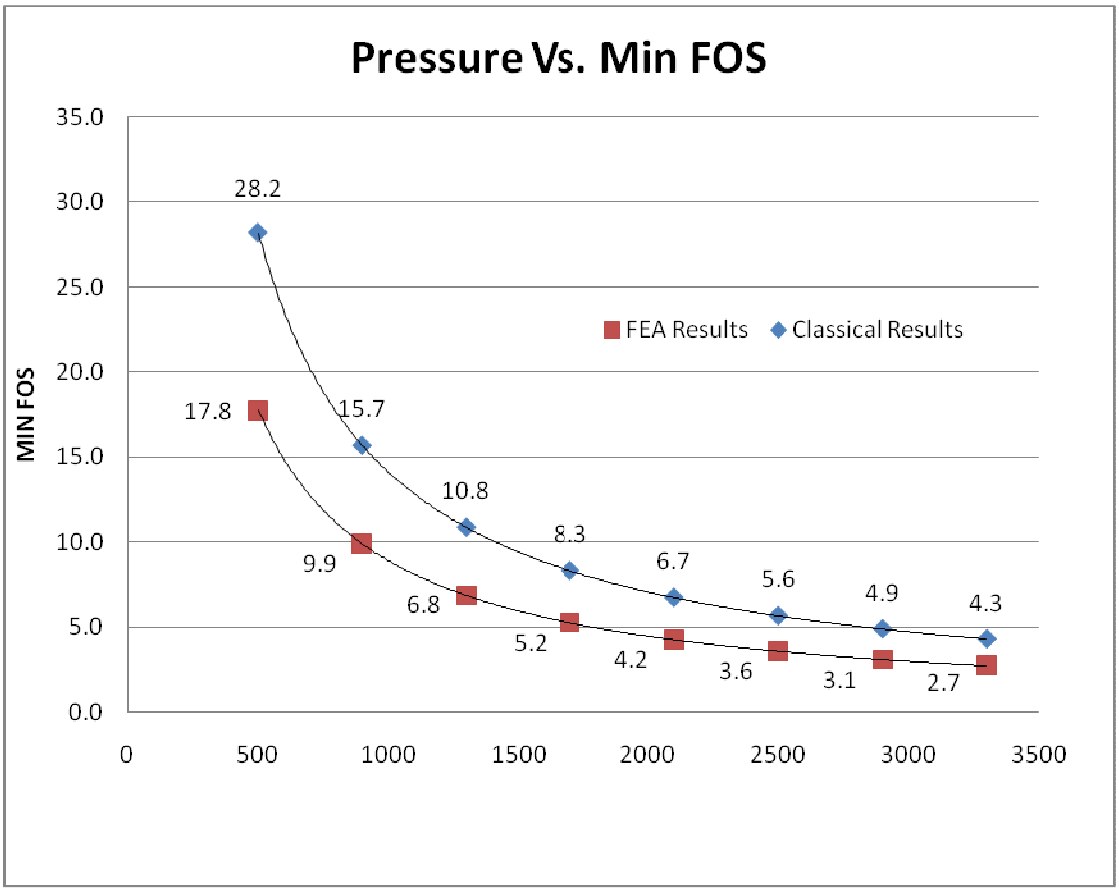

geometry for the combustion vessel. In the case of the classical calculations, a simple

geometry consisting of a pure cylinder with two holes on opposite sides was assumed. The finite element model, however, takes into account variations in the combustion vessel geometry. The differences in the assumed geometries can be seen in Figure x below.

If the combustion vessel rig were to consistently be operated at room temperatures, this analysis would have been finished at this point. Due to the fact that significant heat input was required, however, the effect of heat energy on the structural integrity of the rig was evaluated. This was done using the rules set forth by the ASME Boiler and Pressure Vessel Code. According to the code, the maximum allowable stress for elevated temperature service of pressure vessels is the minimum of the following:

I) $\frac{1}{3.5}$ * UTS at Room Temperature

II) $\frac{1}{4}$ * UTS at Elevated Temperature

III) $\frac{2}{3}$ * YS at Room Temperature

IV) $\frac{2}{3}$ *YS at Elevated Temperature

V) The stress value known to produce creep of 1% in 100,000 hours

VI) $\frac{4}{5}$ * The stress value known to produce failure due to creep in 100,000 hours

For this analysis, the maximum stress seen in the combustion vessel as a function of pressure was coupled with the maximum allowable stress subject to rules I–VI to determine the maximum allowable pressure in the combustion vessel as a function of temperature.

Figure A2 illustrates these six criterion, with the minimum value at a specific temperature corresponding to the maximum allowable pressure. As can be seen in Figure A2, it would be unwise to operate the pressure vessel at a temperature greater than 500 C, due to the potential

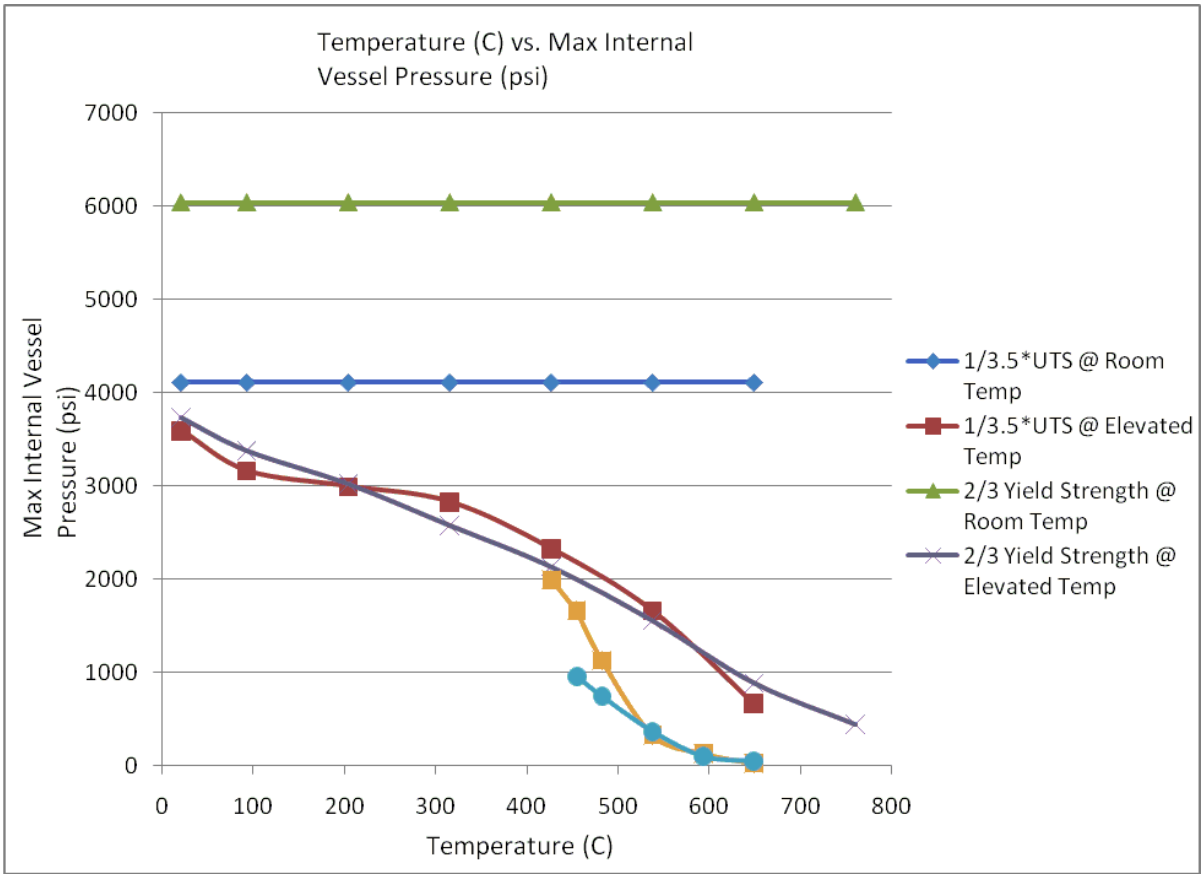

Figure A2: Maximum allowable vessel pressures as a function of temperature

of eventual creep rupture. Because of this, the apparatus is installed with an interior refractory liner, as well as insulation. The purpose of these measures is to inhibit heat transfer, and allow higher temperatures to be achieved in the combustion vessel without exceeding the structural limitations. In order to monitor the vessel temperature, a thermocouple has been installed on the outer edge of the thermal insulation. This temperature is assumed to represent the overall temperature of the metal.

Image Processing Code

```
        CREATE A MATRIX OF ZEROS
B=zeros([1024 1280 1 1],'uint16');
B=zeros([1024 1280 1 25],'uint16');

        READ IN IMAGES-CHOOSE FILENAMES AND QUANTITIES
for frame=1:25
A50(:,:,:,frame),map]=imread('D:\Diesel Injection\ISU Injection\October 2008\500 psi\90
MPA\50 micro.tif',frame);
A250(:,:,:,frame),map]=imread('D:\Diesel Injection\ISU Injection\October 2008\500 psi\90
MPA\250 micro.tif',frame);
A450(:,:,:,frame),map]=imread('D:\Diesel Injection\ISU Injection\October 2008\500 psi\90
MPA\450 micro.tif',frame);
A650(:,:,:,frame),map]=imread('D:\Diesel Injection\ISU Injection\October 2008\500 psi\90
MPA\650 micro.tif',frame);
A850(:,:,:,frame),map]=imread('D:\Diesel Injection\ISU Injection\October 2008\500 psi\90
MPA\850 micro.tif',frame);
A1050(:,:,:,frame),map]=imread('D:\Diesel Injection\ISU Injection\October 2008\500 psi\90
MPA\1050 micro.tif',frame);
end

        BACKGROUND SUBTRACTION & ELIMINATE EXTRANEOUS NOISE
for frame=1:25
A50(:,:,:,frame)=A50(:,:,:,frame)-Background_avg2;
A250(:,:,:,frame)=A250(:,:,:,frame)-Background_avg2;
A450(:,:,:,frame)=A450(:,:,:,frame)-Background_avg2;
A650(:,:,:,frame)=A650(:,:,:,frame)-Background_avg2;
A850(:,:,:,frame)=A850(:,:,:,frame)-Background_avg2;
A1050(:,:,:,frame)=A1050(:,:,:,frame)-Background_avg2;
A50(759:764,193:194,frame)=0;
A250(759:764,193:194,frame)=0;
A450(759:764,193:194,frame)=0;
A650(759:764,193:194,frame)=0;
A850(759:764,193:194,frame)=0;
A1050(759:764,193:194,frame)=0;
end

WRITE PROCESSED .TIF FILES
for frame=1:25
imwrite(A50(:,:,:,frame),'D:\Diesel Injection\ISU Injection\October 2008\500 psi\90
MPA\Processed\50 micro processed.tif','WriteMode','append');
imwrite(A250(:,:,:,frame),'D:\Diesel Injection\ISU Injection\October 2008\500 psi\90
MPA\Processed\250 micro processed.tif','WriteMode','append');
```

```
imwrite(A450(:,:,:,frame),'D:\Diesel Injection\ISU Injection\October 2008\500 psi\90
MPA\Processed\450 micro processed.tif','WriteMode','append');
imwrite(A650(:,:,:,frame),'D:\Diesel Injection\ISU Injection\October 2008\500 psi\90
MPA\Processed\650 micro processed.tif','WriteMode','append');
imwrite(A850(:,:,:,frame),'D:\Diesel Injection\ISU Injection\October 2008\500 psi\90
MPA\Processed\850 micro processed.tif','WriteMode','append');
imwrite(A1050(:,:,:,frame),'D:\Diesel Injection\ISU Injection\October 2008\500 psi\90
MPA\Processed\1050 micro processed.tif','WriteMode','append');
end

EVALUATE PENETRATION DISTANCE-CHOOSE INTERROGATION REGION AND
SENSITIVIY

for frame=1:25
        for row=60:200
                for col=560:780
                        B50(1,(col-559),frame)=A50(row,col,frame);
                        continue
                end

                        [c]=find(B50>60);
                        test=isempty([c]);

                        if test==0;
                                penetration50(frame,1)=row-59;
                                continue
                        else
                        end
        end
end

WRITE EXCEL FILES-FILENAMES, MATRICES TO WRITE, WORKSHEET NAME,
COLUMN LOCATIONS

xlswrite('D:\Diesel Injection\ISU Injection\October 2008\500 psi\Centerline PD_s
Hi_Press',penetration50,'90 MPa','B3:B27');
xlswrite('D:\Diesel Injection\ISU Injection\October 2008\500 psi\Centerline PD_s
Hi_Press',penetration250,'90 MPa','C3:C27');
xlswrite('D:\Diesel Injection\ISU Injection\October 2008\500 psi\Centerline PD_s
Hi_Press',penetration450,'90 MPa','D3:D27');
xlswrite('D:\Diesel Injection\ISU Injection\October 2008\500 psi\Centerline PD_s
Hi_Press',penetration650,'90 MPa','E3:E27');
xlswrite('D:\Diesel Injection\ISU Injection\October 2008\500 psi\Centerline PD_s
Hi_Press',penetration850,'90 MPa','F3:F27');
```

```
xlswrite('D:\Diesel Injection\ISU Injection\October 2008\500 psi\Centerline PD_s
Hi_Press',penetration1050,'90 MPa','G3:G27');


        FOR FILE "D:\Diesel Injection\100 shot cuvette 266nm.tif\"

Norm=zeros([844 30 1 100],'uint16');
NormRows=zeros([844 1 1 100],'uint16');

for frame=1:20
        for row=140:765
                for col=711:947
                        spray_eval(row-139,col-710,frame)=spray(row,col,frame);
                        continue
                end
                continue
        end
continue
end
```

ACKNOWLEDGEMENTS

Graduate school was a truly unique experience for me. I would first like to thank my advisor, Dr. Terrence Meyer, for the opportunity to work in such a unique environment. I would also like to thank Dr. Meyer for maintaining a highly enjoyable atmosphere to work in. I would like to thank Dr. Song-Charng Kong, Anthony Phan, and all of the other graduate students in Dr. Kong's group for their support. I would also like to thank Jim Dautremont and Larry Couture for their support and advice. In addition, none of the work for this project would have been possible without the support of engineers at John Deere. Finally, I would like to thank the other graduate students in Dr. Meyer's group for both their support and friendship during my time as a graduate student at Iowa State.